Electromagnetic Studies and Subsurface Mapping of Electrical Resistivity in the La Bajada Constriction Area, New Mexico

By Brian D. Rodriguez, Maria Deszcz-Pan, and David A. Sawyer

Chapter F of

The Cerrillos Uplift, the La Bajada Constriction, and Hydrogeologic Framework of the Santo Domingo Basin, Rio Grande Rift, New Mexico

Edited by Scott A. Minor

Professional Paper 1720–F

U.S. Department of the Interior
U.S. Geological Survey

Contents

Figures

Tables

Electromagnetic Studies and Subsurface Mapping of Electrical Resistivity in the La Bajada Constriction Area, New Mexico

By Brian D. Rodriguez, Maria Deszcz-Pan, and David A. Sawyer

Abstract

Airborne and surface electromagnetic surveys were used to map changes in electrical resistivity with depth in the La Bajada constriction and Cochiti Pueblo area; these changes in resistivity are related to variations in rock or deposit types that, in turn, influence aquifers in the study area. In the eastern Cerros del Rio volcanic field, the location and geometry of the northern boundary of the Cerrillos uplift are constrained by our electromagnetic survey results. This boundary defines the southeastern extent of the La Bajada constriction through which groundwater hydraulically connected with the Rio Grande flows as it passes from the Española Basin into the Santo Domingo Basin. The largely concealed Tetilla fault zone is also detected by the electromagnetic surveys in this area; it appears to form the western boundary of an east-dipping block of electrically conductive Mancos Shale. In the north-central part of the La Bajada constriction, a large area of lower resistivity coincides with a silt or clay lacustrine unit in upper Santa Fe Group basin-fill deposits. In the central part of the constriction, higher resistivities correspond in part with ancestral Rio Grande axial gravel deposits. On the western flank of the La Bajada constriction, our electromagnetic survey results provide constraints on the relative position of basement and on the thicknesses of Paleozoic, Mesozoic, and Tertiary sedimentary rocks on either side of the constriction-bounding Pajarito fault zone.

Introduction to Electromagnetic Methods

Studies by the U.S. Geological Survey were begun in 1996 to improve understanding of the geologic framework of the Albuquerque composite basin and adjoining areas, in order that more accurate hydrogeologic parameters could be applied to new hydrologic models. The ultimate goal of this multidisciplinary effort has been to better quantify estimates of future water supplies for northern New Mexico's growing urban centers, which largely subsist on aquifers in the Rio Grande rift basin (Bartolino and Cole, 2002). From preexisting hydrologic models it became evident that hydrogeologic uncertainties were large in the Santo Domingo Basin area, immediately upgradient from the greater Albuquerque metropolitan area, and particularly in the northeast part of the basin referred to as the La Bajada constriction (see chapter A, this volume, for a geologic definition of this feature as used in this report). Accordingly, a priority for new geologic and geophysical investigations was to better determine the hydrogeologic framework of the La Bajada constriction area. This chapter along with the other chapters of this report present the results of such investigations recently conducted by the U.S. Geological Survey.

Airborne and surface electromagnetic (EM) surveys are described here as part of U.S. Geological Survey investigations of the subsurface distribution of sedimentary and volcanic rocks in the Cochiti Pueblo and La Bajada constriction areas (survey area D, fig. F1). An airborne time-domain electromagnetic (TDEM) survey was used to map changes in electrical resistivity with depth that are related to differences in rock type; these various rock types, in turn, affect the hydrologic properties of aquifers in the region. A ground-based magnetotelluric (MT) survey was used to calibrate TDEM results and to obtain electrical resistivity information from depths greater than the limits of the TDEM survey. In this chapter we discuss the electrical rock property called resistivity, the surface (MT) and airborne (TDEM) electromagnetic methods used in our study, and our approach to modeling and interpreting MT and TDEM data. We present subsurface maps and cross sections of resistivity and interpret the basic geologic framework of the study area on the basis of these data.

Electrical Rock Properties

Electromagnetic geophysical methods detect variations in the electrical properties of rocks—in particular electrical resistivity (or its inverse, electrical conductivity). Electrical resistivity can be correlated with geologic units on the surface and at depth by using lithologic logs to provide a three-dimensional picture of subsurface geology. The resistivity of geologic units largely depends on their fluid content,

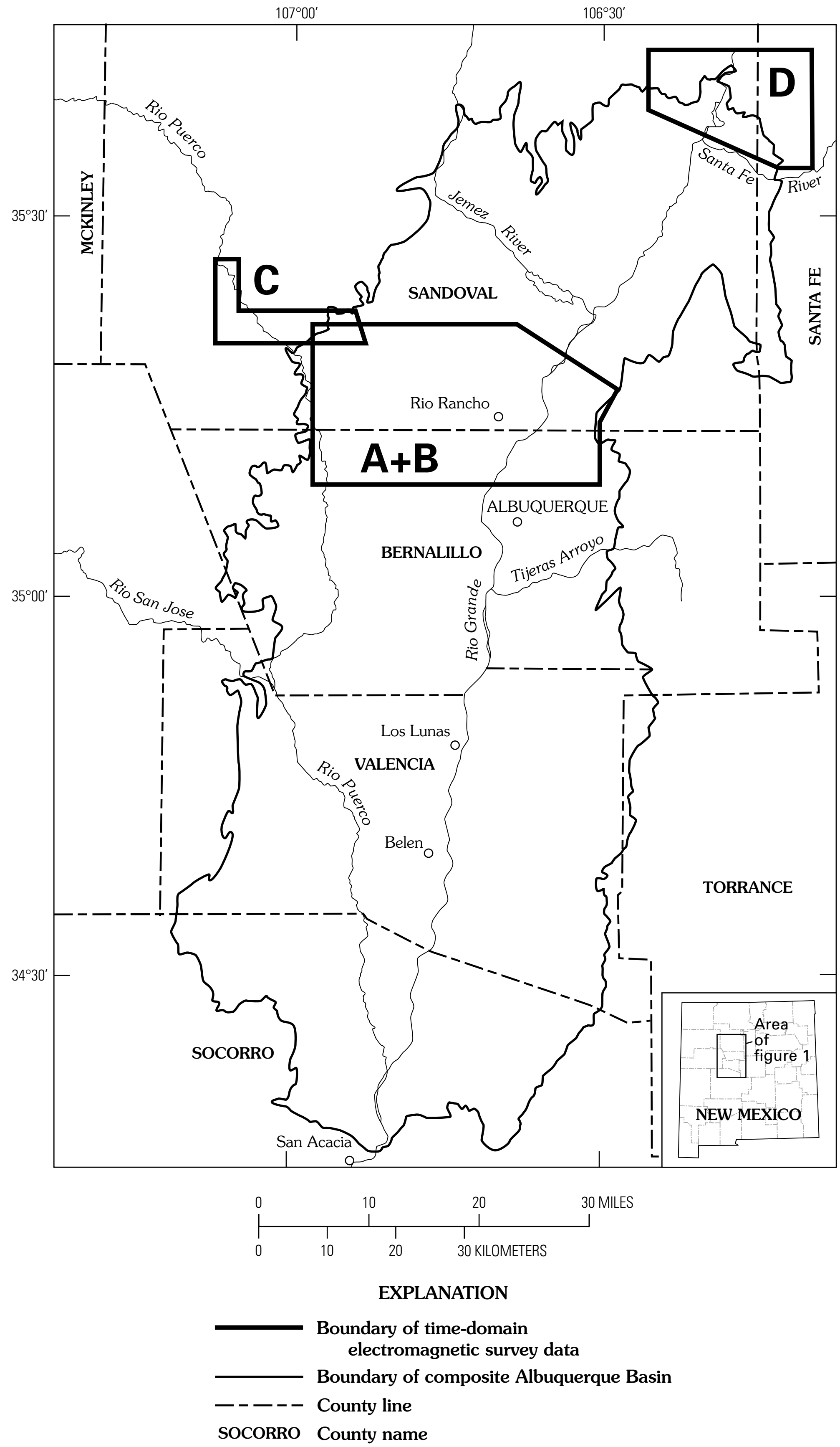

Figure F1. Airborne time-domain electromagnetic survey areas in the middle Rio Grande Basin north of Albuquerque, New Mexico, modified from Bartolino (1999). A+B, Rio Rancho survey area. C, Rio Puerco survey area, both described in Deszcz-Pan and others (2000). D, Cochiti Pueblo survey area discussed in this chapter.

porosity, fracture density, temperature, and content of conductive minerals (Keller and Frischknecht, 1966). Fluids in the pore spaces and fracture openings, especially saline fluids, can reduce resistivities in what would otherwise be a resistive rock matrix. Resistivity can also be lowered by electrically conductive clay minerals, graphitic carbon, and deposits of metallic minerals. Altered volcanic rocks commonly contain replacement minerals that have resistivities that are only a tenth of the resistivities of minerals in unaltered surrounding rocks (Nelson and Anderson, 1992). Water-saturated clay-rich alluvium, marine shale, and other mudstones are normally very conductive—a few (1–3) ohms per meter to a few tens (10–20) of ohms per meter. Water-saturated, unconsolidated, terrestrial alluvial sediments are commonly moderately conductive (10–70 ohm-m). Sediments containing conglomerate and coarse, clean sand possess resistivities at the higher end of the range, and impure sand and siltstone lie at the lower end. The resistivity of water-saturated unconsolidated sediment, at low temperature and measured at low frequencies, is controlled by the relative proportion of clay minerals, porosity, interconnected pore structures, and dissolved minerals (Keller, 1987; Palacky, 1987).

Unaltered, unfractured igneous rocks are normally very resistive (typically a few hundred to thousands of ohm-m). Carbonate rocks are moderately to highly resistive (hundreds to thousands of ohms per meter) depending upon their fluid content, porosity, fracture characteristics, and impurities. Metamorphic rocks (that do not contain graphite) are moderately to highly resistive (hundreds to thousands of ohms per meter). Resistivity may be low (less than 100 ohm-m) along fault zones that were fractured enough to have once hosted fluids (generally water or brine) from which conductive minerals were deposited. Higher subsurface temperatures cause greater mobility of ions in the fluids and increase the energy level above the activation energy for electrons or ions, factors that considerably reduce rock resistivity (Keller and Frischknecht, 1966). Tables of electrical resistivity for a variety of rocks, minerals, and geologic environments may be found in Keller (1987) and Palacky (1987).

Ground-Based Electromagnetic Surveys

The MT method is a passive ground-based electromagnetic geophysical technique that investigates the distribution of electrical resistivity (or its inverse, electrical conductivity) below the surface at depths of tens of meters to tens of kilometers (Vozoff, 1991). It does so by measuring the Earth's natural electric and magnetic fields. Worldwide lightning activity at frequencies of 10,000 to 1 hertz (Hz) and geomagnetic micropulsations at frequencies of 1 to 0.001 Hz provide the main frequency bands used by the MT method. The natural electromagnetic waves propagate vertically in the Earth because the very large contrast in the resistivity of the air and the Earth causes a vertical refraction of the electromagnetic wave at the Earth's surface (Vozoff, 1972).

The natural electric and magnetic fields are recorded in two orthogonal, horizontal directions (the vertical magnetic field is also recorded). The resulting time-series signals are used to derive Earth-tensor apparent resistivities and phases after first converting them to complex cross-spectra using fast Fourier transform techniques and least-squares, cross-spectral analysis (Bendat and Piersol, 1971) to solve for a tensor transfer function. If one assumes that the Earth consists of a two-input, two-output, linear system in which the orthogonal magnetic fields are input and the orthogonal electric fields are output, then the calculated function relates the observed electric fields to the magnetic fields. Before it is converted to apparent resistivity and phase, the tensor is normally rotated into principal directions that usually correspond with the direction of maximum and minimum apparent resistivity. For a two-dimensional Earth, the MT fields can be decoupled into transverse electric and transverse magnetic modes. Two-dimensional resistivity modeling is generally computed to fit both modes. When the geology satisfies the two-dimensional assumption, the MT data for the transverse electric mode are assumed to represent the electric field along geologic strike, and the data for the transverse magnetic mode are assumed to represent the electric field across strike. The MT method is well suited for studying complicated geologic environments because the electric and magnetic relations are sensitive to vertical and horizontal variations in resistivity. The method is capable of establishing whether the electromagnetic fields are responding to subsurface rock bodies of effectively one, two, or three dimensions. An introduction to the MT method and references for a more advanced understanding are contained in Dobrin and Savit (1988) and Vozoff (1991).

Magnetotelluric Survey

Six high-frequency MT soundings (stations 1–6, table F1) were acquired in 1997 in the Cochiti Pueblo survey area (figure F2*A*). Spacing between soundings ranged from 4.5 to 11 km. Some stations were used to calibrate the inversion of the airborne TDEM data. These stations were located in areas that had a locally one-dimensional TDEM response and were close to roads but distant from sources of electrical noise, such as power lines. Horizontal electric fields were sensed using titanium electrodes placed in an L-shaped, three-electrode array with dipole lengths of 30 m. The orthogonal, horizontal magnetic fields in the direction of the electric-field measurement array were sensed using high magnetic permeability, mu-metal-cored (80 percent nickel, 15 percent iron, 5 percent molybdenum) induction coils. Frequencies sampled ranged from 20,000 to 4 Hz by use of single-station recordings of both orthogonal horizontal components of the electric and magnetic fields and of the vertical magnetic field. These frequencies lie at the high end of the MT spectrum and are commonly referred to as audiomagnetotelluric (AMT) frequencies. Sampling these frequencies in the Cochiti Pueblo allowed us to probe the subsurface from depths of tens of meters to about one kilometer (Williams, Rodriguez, and Sampson,

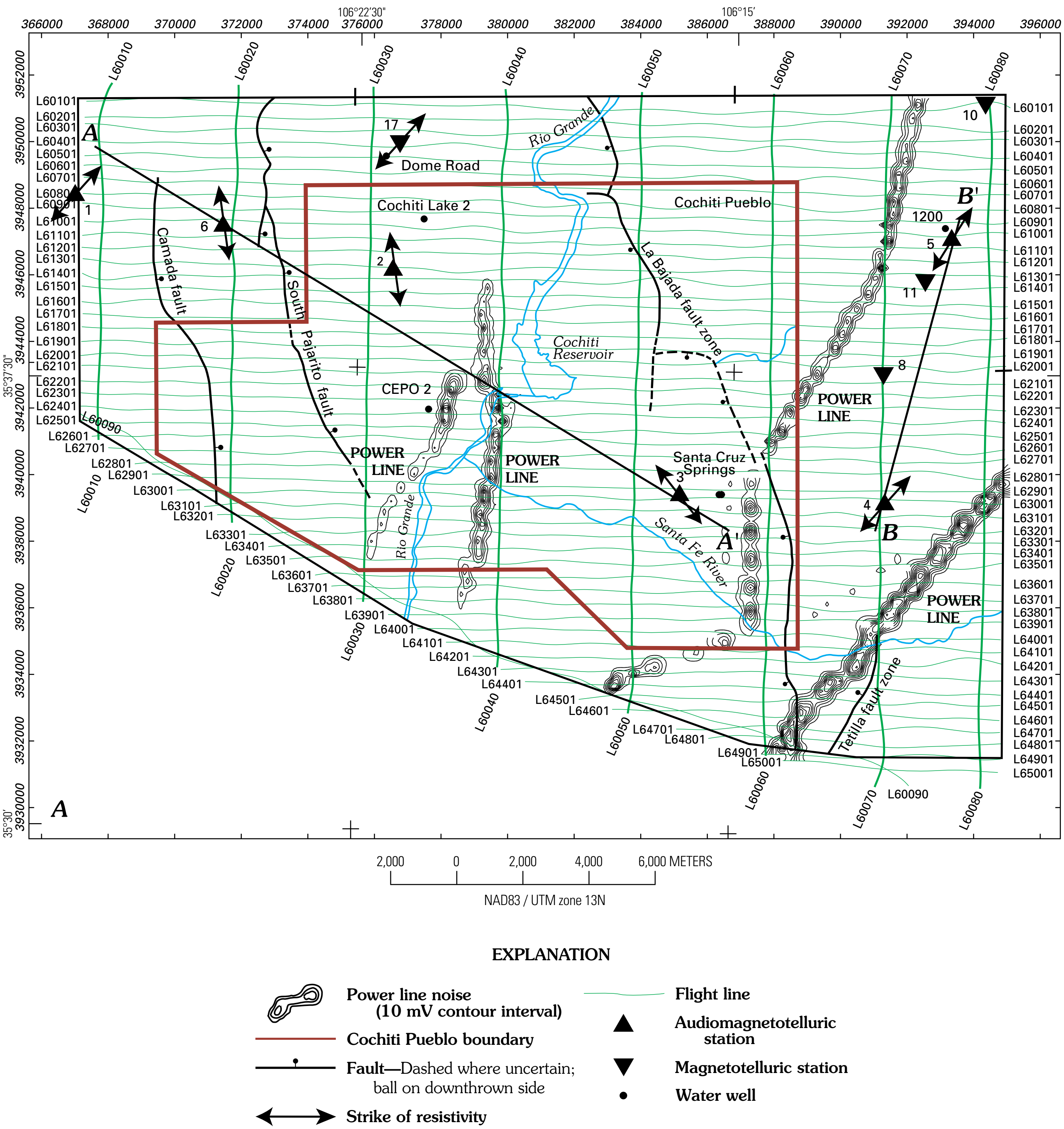
106°22'30"
106°15'
366000
368000
370000
372000
374000
376000
378000
380000
382000
384000
386000
388000
390000
392000
394000
396000
3952000
3950000
3948000
3946000
3944000
3942000
3940000
3938000
3936000
3934000
3932000
3930000
35°37'30"
35°30'
L60010
L60020
L60030
L60040
L60050
L60060
L60070
L60080
L60090
A
A'
B
B'
1
2
3
4
5
6
8
10
11
17
1200
Dome Road
Cochiti Lake 2
Cochiti Pueblo
Rio Grande
Cochiti Reservoir
CEPO 2
Camada fault
South Pajarito fault
La Bajada fault zone
Tetilla fault zone
Santa Cruz Springs
Santa Fe River
POWER LINE
2,000 0 2,000 4,000 6,000 METERS
NAD83 / UTM zone 13N
EXPLANATION
Power line noise (10 mV contour interval)
Cochiti Pueblo boundary
Fault—Dashed where uncertain; ball on downthrown side
Strike of resistivity
Flight line
Audiomagnetotelluric station
Magnetotelluric station
Water well

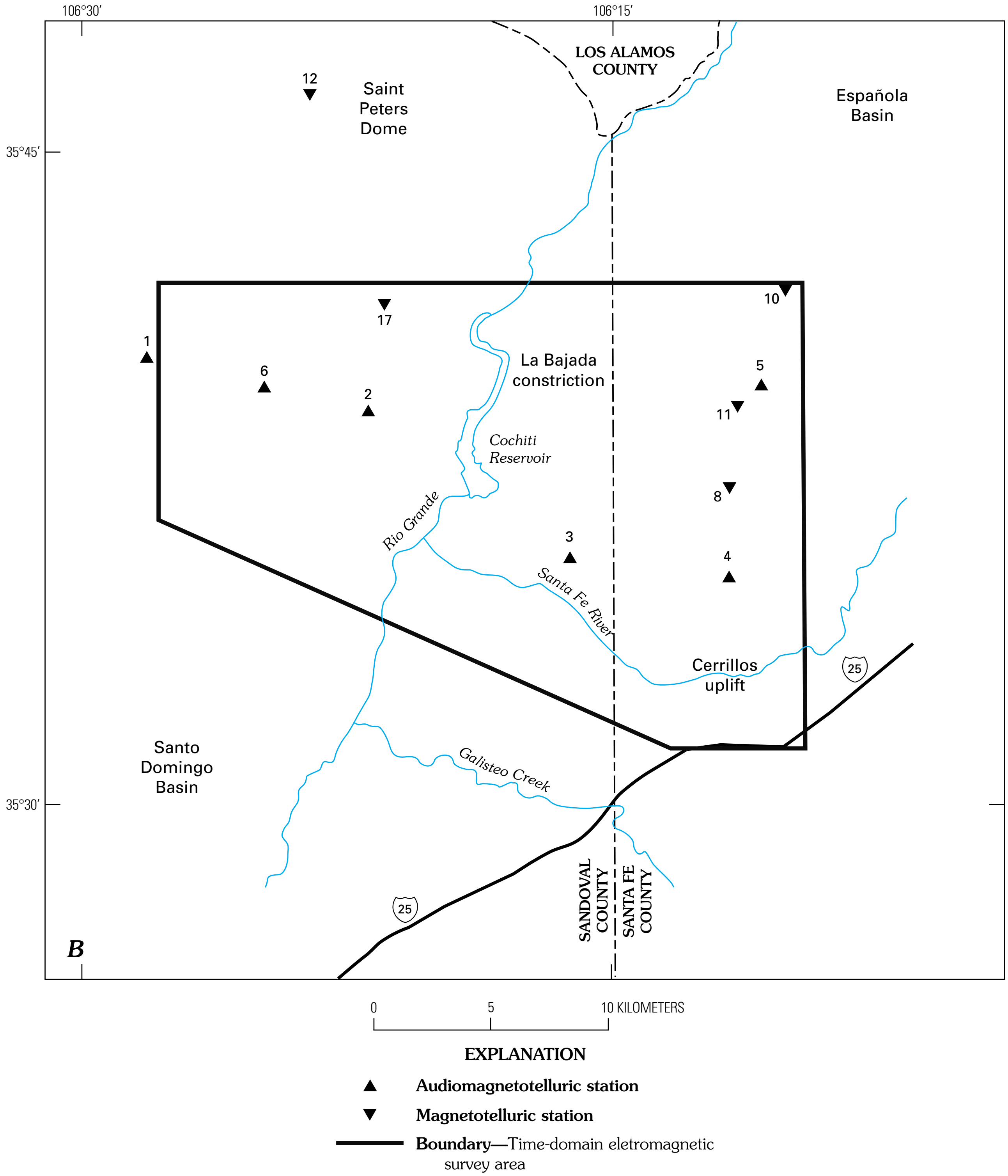

Figure F2 (above and facing page). Cochiti Pueblo time-domain electromagnetic survey area (survey area D, fig. F1) northeast of Albuquerque, New Mexico. High-frequency magnetotelluric (AMT) sounding stations 1–6 acquired in 1997; low-frequency magnetotelluric (MT) sounding stations 8, 10, 11, 12, and 17 acquired in 2002. *A*, Flight lines flown in airborne time-domain electromagnetic survey. *B*, Location of AMT and MT stations. The La Bajada constriction contains Santa Fe Group basin-fill sedimentary aquifers linking the Española and Santo Domingo Basins. Cerrillos uplift constrained by gravity data (chapter D, this volume) and by AMT stations 4 and 5 and MT stations 8, 10, and 11.

2001). Five low-frequency MT soundings (table F1) were also acquired in 2002 in the survey area (sites 8, 10, 11, 12 and 17), fig. F2*B*.

The recorded time-series data were transformed to the frequency domain using Fourier analysis to determine a two-dimensional apparent resistivity and phase tensor at each site. The data were rotated to maximum and minimum apparent resistivity directions so that propagation modes for the signals were decoupled into transverse electric and transverse magnetic modes. This treatment supplies the local strike of electrical sources (illustrated by double-headed arrows in fig. F2*A*). Local reference sensors were used to help reduce bias in the determinations of impedance that otherwise would be caused by noise in the instruments or the environment (Gamble, Goubau, and Clarke, 1979; Clarke and others, 1983). We also sorted cross-power files to select optimal signal-to-noise data sets. Figure F3*A*, *B* shows observed data represented by digitized values of the transverse electric and transverse magnetic modes from the AMT soundings after the raw data curves were smoothed (Williams, Rodriguez, and Sampson, 2001).

The effects of near-surface resistivity anomalies can cause "static shifts" (Sternberg, Washburne, and Pellerin, 1988) in the data. Such shifts are minor in most of this data set. Only at station 4 was a static shift larger than one-third of a log decade. At the remaining stations very minor static shifts ranged from 0.0 to less than 0.3 of a log decade. Only the large static shifts were accounted for in subsequent two-dimensional modeling of the data.

Resistivity Models Based on Magnetotelluric Survey

The AMT data were modeled by use of a two-dimensional finite-element resistivity algorithm (Wannamaker, Stodt, and Rijo, 1985) called PW2D. The two-dimensional resistivity model is constructed by adjusting the resistivity values beneath the profile of AMT stations, so that for all stations the calculated two-dimensional response agrees with the measured data. From our six AMT stations, we constructed two profiles. Profile A-A′ (fig. F2*A*), at a bearing of N. 70° W., passes directly through AMT stations 6 and 3. AMT stations 1 and 2 are projected more than 1 km north and south, respectively, onto the line A-A′. The profile B-B′ (fig. F2*A*) lies between AMT stations 4 and 5 at a bearing of N. 15° E. The finite-element grid used in these models consisted of 51×26 variable-dimension cells that extended 10 km horizontally beyond the profile end points and 2 km

Figure F3 (facing and following 2 pages). Observed and computed data used to generate two-dimensional finite-element resistivity models (figs. F4*A*, F5, F6) in the Cochiti Pueblo time-domain electromagnetic survey area (area D, fig. F2). *A*, High-frequency magnetotelluric (AMT) observed apparent resistivity data. *B*, AMT observed apparent phase data. *C*, Low-frequency magnetotelluric (MT) observed apparent resistivity data. *D*, MT observed apparent phase data.

Table F1. Audiomagnetotelluric and magnetotelluric station coordinates and elevations in the Cochiti Pueblo area, New Mexico.

[Coordinates are referenced to the 1866 Clarke spheroid and North American 1927 Western United States datum; stations listed in order from west to east; locations determined by use of a global positioning system; longitude and latitude format is in decimal degrees. AMT, audiomagnetotelluric; MT, magnetotelluric; UTM, Universal Transverse Mercator]

Station	Type of sounding	Longitude	Latitude	UTM (m)		Elevation	
				North	East	(m)	(ft)
1	AMT	–106.46612	35.67263	3,948,430	13,367,310	2,063	6,768
6	AMT	–106.41874	35.66382	3,947,390	13,371,585	1,760	5,774
12	MT	–106.38889	35.76750	3,958,861	13,374,449	2,380	7,808
2	AMT	–106.36313	35.65193	3,946,000	13,376,600	1,740	5,709
17	MT	–106.36167	35.68583	3,949,770	13,376,785	1,750	5,741
3	AMT	–106.26918	35.59192	3,939,230	13,385,020	1,657	5,436
4	AMT	–106.20242	35.58593	3,938,490	13,391,060	1,903	6,243
8	MT	–106.20222	35.62361	3,942,655	13,391,127	2,020	6627
5	AMT	–106.17803	35.66128	3,946,820	13,393,370	2,045	6,709
11	MT	–106.18861	35.64639	3,945,184	13,392,391	2,025	6,644
10	MT	–106.16806	35.69806	3,950,901	13,394,319	2,170	7,119

A

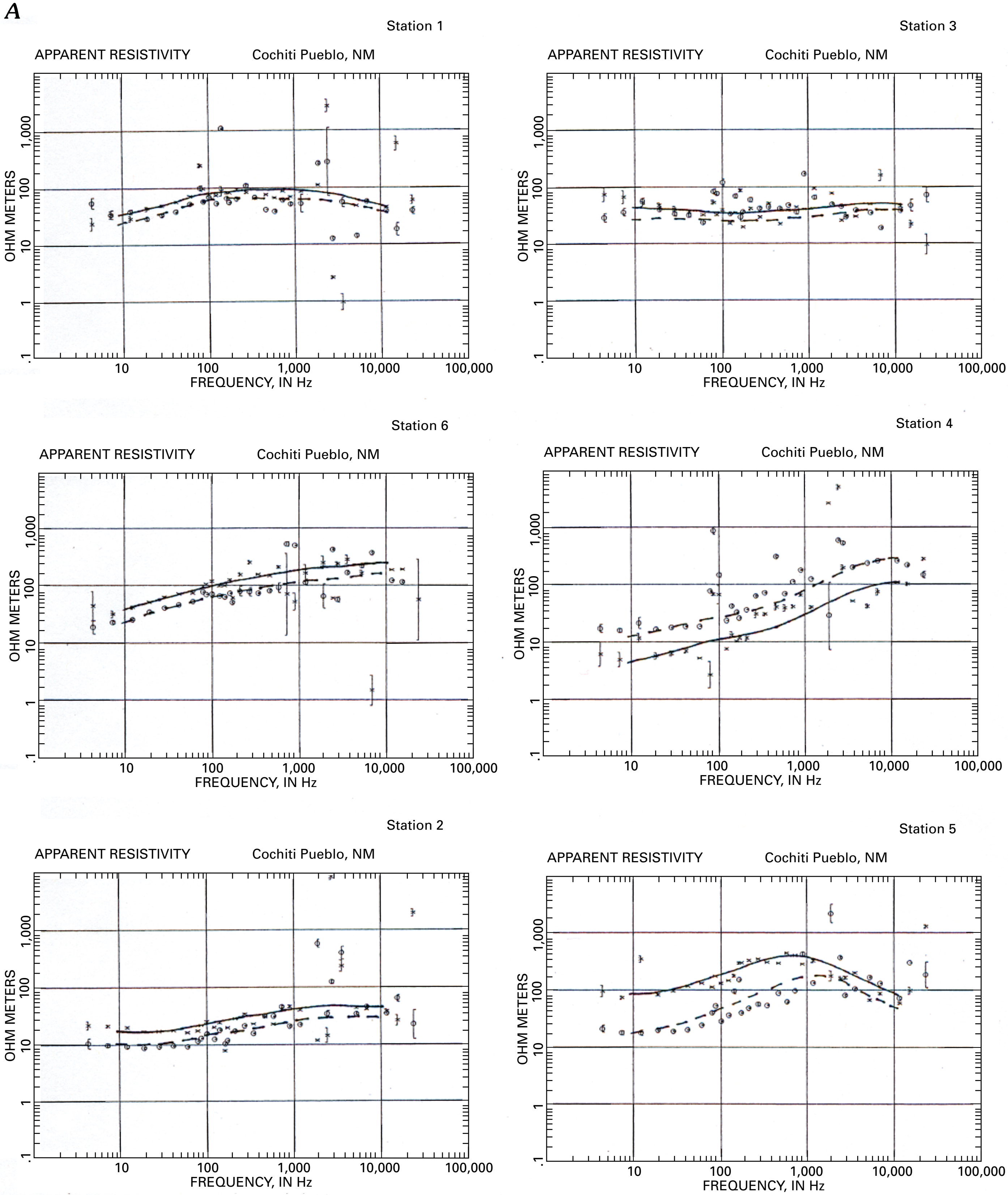

EXPLANATION

x Observed transverse electric data	[Observed transverse magnetic error
o Observed transverse magnetic data	——— Computed transverse electric data
] Observed transverse electric error	— — — Computed transverse magnetic data

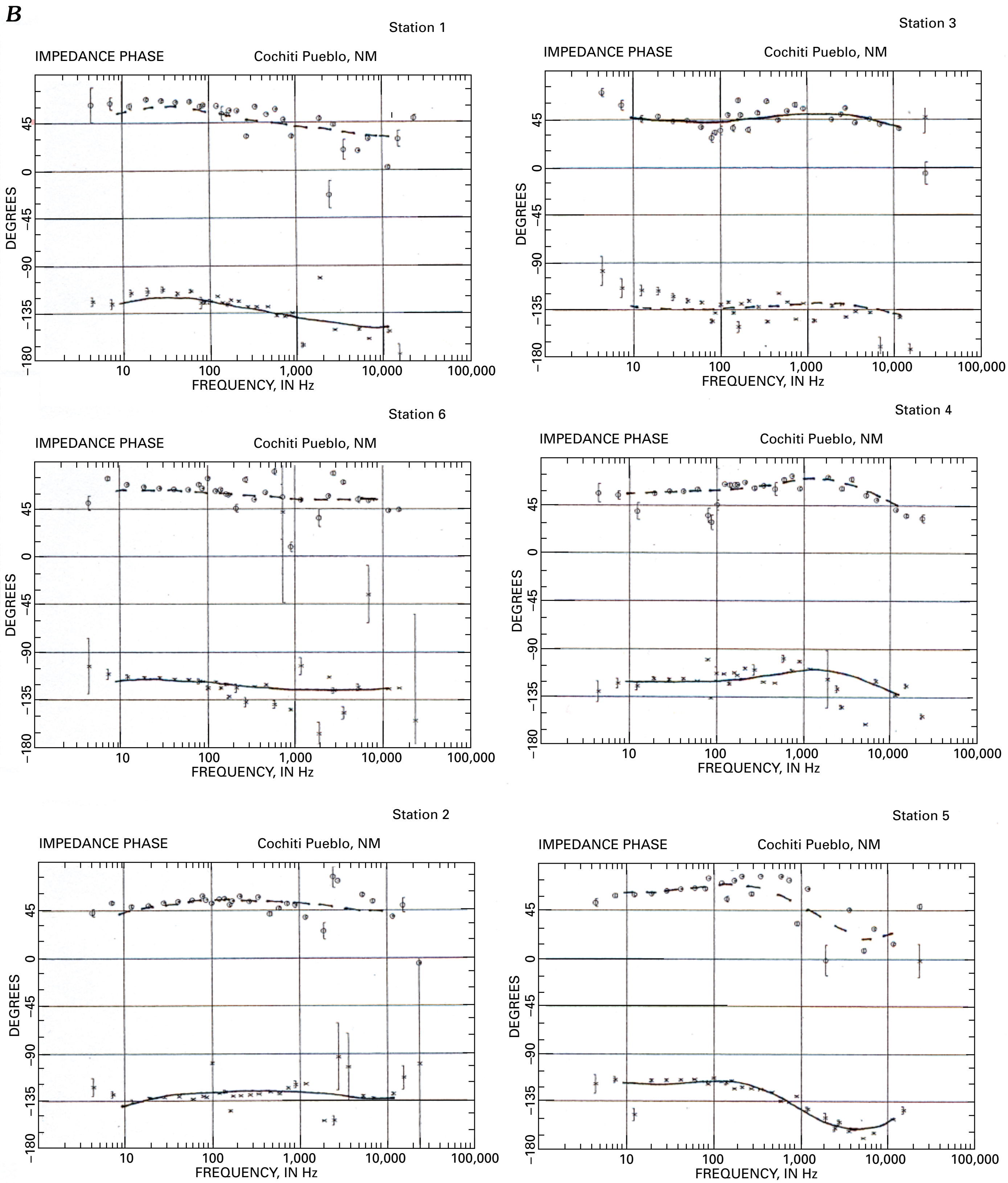

EXPLANATION

x	Observed transverse electric data	[	Observed transverse magnetic error
o	Observed transverse magnetic data	———	Computed transverse electric data
]	Observed transverse electric error	— — —	Computed transverse magnetic data

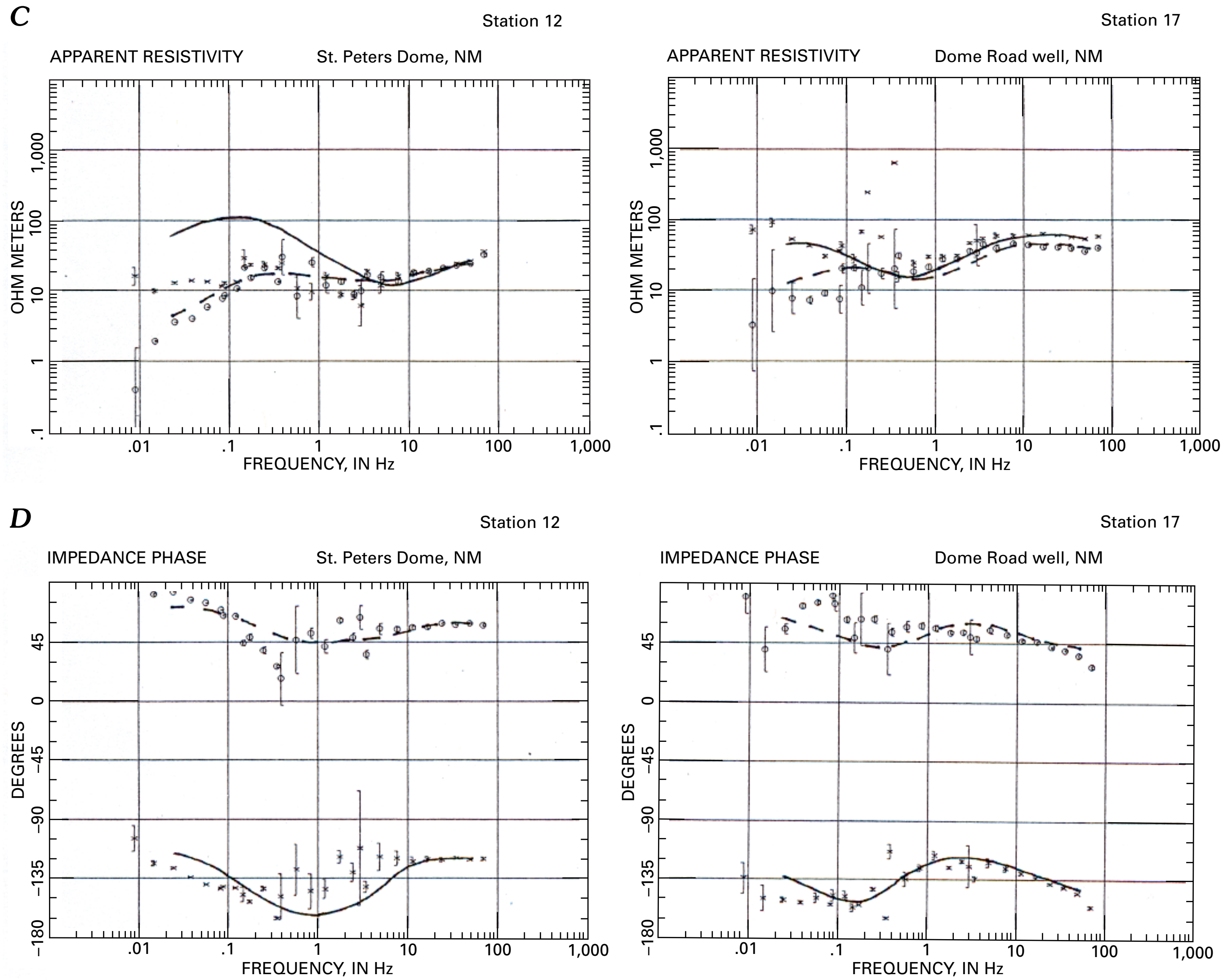

EXPLANATION

x	**Observed transverse electric data**	[	**Observed transverse magnetic error**
o	**Observed transverse magnetic data**	———	**Computed transverse electric data**
]	**Observed transverse electric error**	— — —	**Computed transverse magnetic data**

vertically to minimize edge effects. In the finer part of the mesh, the size of the horizontal element ranged between 500 and 1,000 m. The size of the vertical element ranged from 5 m near the surface to 300 m below 1 km depth. We forward modeled by perturbing each two-dimensional model (figs. F4*A*, F5) in an attempt to derive the best-fitting calculated response to the transverse electric and transverse magnetic observed responses. Most of the vertical boundaries in the resistivity model represent the minimum widths of a resistive body needed by the AMT data beneath the AMT station. These vertical boundaries generally could be moved 500 m or more in the direction indicated by horizontal arrows in figures F4*A* and F5. The deepest horizontal layer beneath each station in the resistivity model represents the minimum thickness that the layer must have to fit the lowest frequencies of the AMT data.

The MT data were also modeled with program PW2D. The finite-element grid used in these models consisted of 108×70 variable dimension cells that extend 3,000 km horizontally beyond the profile end points and 350 km vertically to minimize edge effects. In the finer part of the mesh, the horizontal element size was 140 m. The vertical element size ranged from 2.5 m near the surface to 1 km below 5 km depth. We forward modeled each two-dimensional model (fig. F6) in an attempt to fit the calculated response to the transverse electric- and transverse magnetic-mode observed responses. Two stations were exceptions: we did not attempt to fit the transverse electric mode below 0.1 Hz at station 12 or below 0.03 Hz at station 17, because the observed data indicated a three-dimensional response (Williams and Rodriguez, 2003). At these frequencies, we primarily attempted to fit the transverse magnetic mode data (Wannamaker, Hohmann, and Ward, 1984).

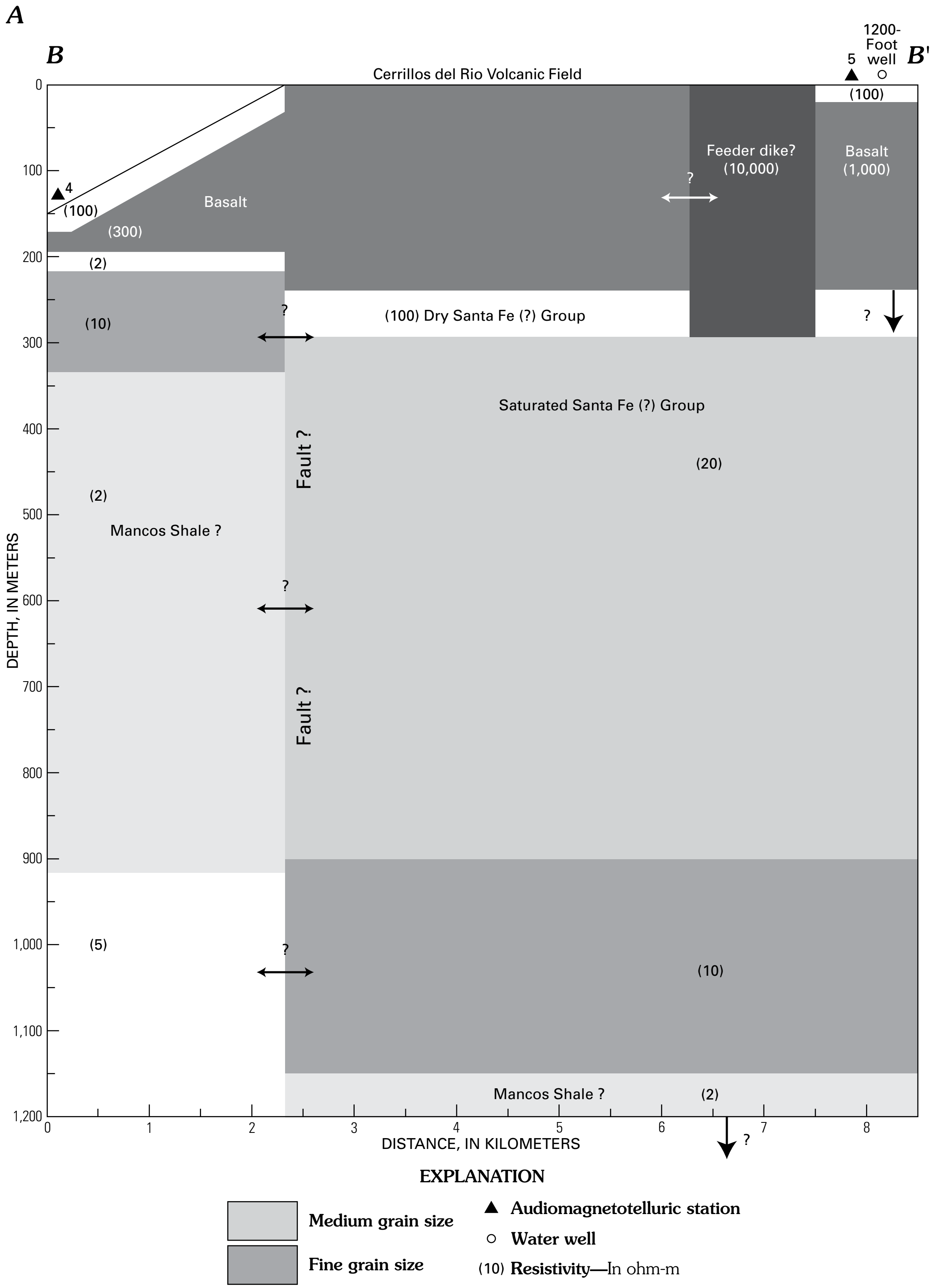
A
B
B'
1200-
Foot
well
5
4
Cerrillos del Rio Volcanic Field
(100)
Basalt
(300)
(2)
(10)
(100) Dry Santa Fe (?) Group
Feeder dike?
(10,000)
Basalt
(1,000)
(100)
?
Saturated Santa Fe (?) Group
(20)
Fault ?
Fault ?
(2)
Mancos Shale ?
(5)
(10)
Mancos Shale ?
(2)
DEPTH, IN METERS
0
100
200
300
400
500
600
700
800
900
1,000
1,100
1,200
DISTANCE, IN KILOMETERS
0
1
2
3
4
5
6
7
8
EXPLANATION
Medium grain size
Fine grain size
Audiomagnetotelluric station
Water well
(10) Resistivity—In ohm-m

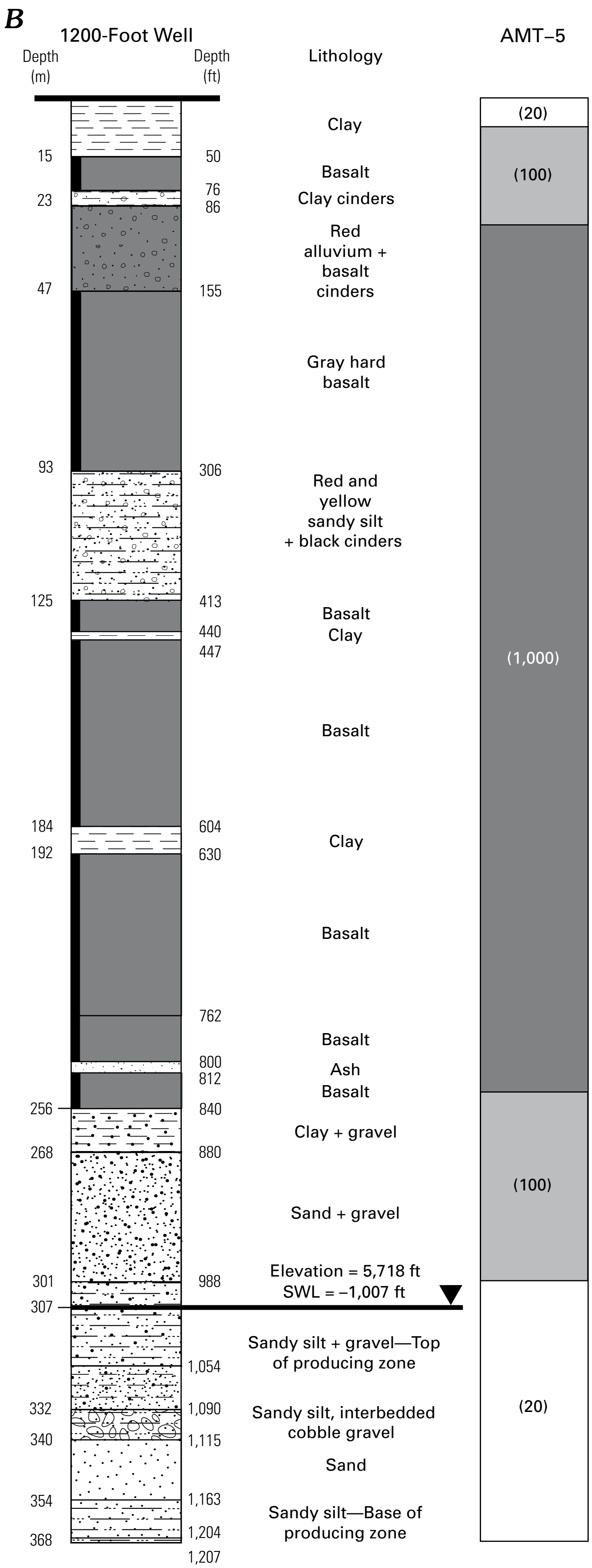

Figure F4 (left and facing page). *A*, Two-dimensional finite-element resistivity model (with lithologic interpretation) constructed from high-frequency magnetotelluric (AMT) data for the Cerros del Rio volcanic field profile B-B′ (fig. F2*A*) in the Cochiti Pueblo time-domain electromagnetic survey area. Arrows within the model indicate uncertainty in the placement of boundaries. Vertical exaggeration is 10. *B*, Comparison of the resistivity model of AMT data at station 5 (fig. F4*A*) and lithology of the 1200-Foot well. Locations of AMT station 5 and 1200-Foot well shown on figure F2*A*.

The calculated fits of our two-dimensional resistivity models (figs. F4*A*, F5, F6) are shown in figure F3. Resistivity boundaries in the model are only approximate because all of the AMT stations are separated by more than 1 km, and the MT stations are separated by more than 8 km. Because of the wide spacing of stations, undetected rock units or structures may exist between stations that are not identified in the resistivity model.

Geologic Interpretation of Surface Electromagnetic Models

Geologic interpretations are based on the resistivity structures revealed in the modeled AMT and MT data (figs. F4*A*, F5, F6) and on regional induction log resistivities of saturated geologic units in seven wells (tables F2, F3): Dome Road (fig. F2*A*), CEPO 2 (fig. F2*A*), Pelto Ortiz 1 (fig. A3), Pelto Blackshare 1 (fig. A3), Black Oil Ferrill 5 (fig. A3), Transocean McKee 1 (fig. A3), and Shell Laguna Wilson Trust 1 (south of our survey area). The northerly electrical strike directions in figure F2*A* can be considered a function of the prominent structural grain of those geologic units, the approximate trend of the shallow geologic structure near the AMT stations (figs. F4*A*, F5), and the approximate structural trend in the upper few kilometers of crust near the MT stations (fig. F6).

As described in chapter A (this volume), the Cochiti Pueblo study area is subdivided into three principal geologic terranes: the western Saint Peters Dome uplifted block, the central subsided La Bajada constriction, and the eastern Cerrillos uplift (fig. A4). AMT and MT stations 1 and 12 are in the western part of the Saint Peters Dome block, in volcanic rocks of the southeastern Jemez volcanic field; stations 2, 3, 6, and 17 are in the northeast part of the Santo Domingo Basin in the central part of the La Bajada constriction; and stations 4 and 5 lie along the northern border of the Cerrillos uplift (figs. F2*B*, A4).

The south-north profile, B-B′ (fig. F2*A*), in the eastern Cerros del Rio volcanic field terrane, shows a moderately resistive basalt (100–300 ohm-m) exposed at the surface that has a thickness of 60±10 m beneath station 4 (fig. F4*A*). Beneath the basalt, a very conductive interval (3 ohm-m) that is 20±10 m thick may be a lacustrine mudstone sequence in

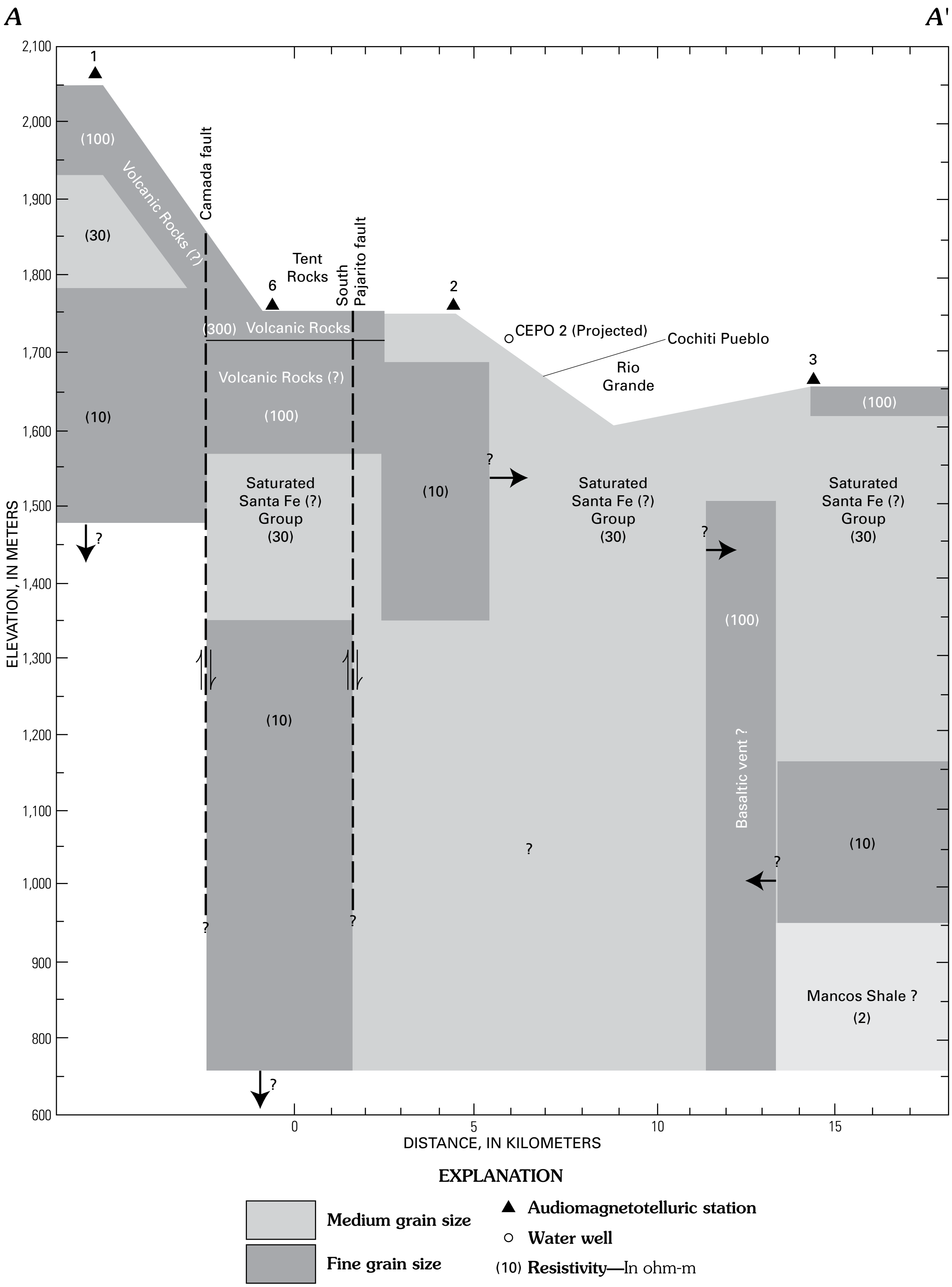

Figure F5. Two-dimensional finite-element resistivity model (with lithologic interpretation) from high-frequency magnetotelluric (AMT) data for the Cochiti Pueblo profile (A-A′, fig. F2*A*) in the Cochiti Pueblo time-domain electromagnetic survey area. Arrow near question mark within the model indicates uncertainty in placement of boundary. Vertical exaggeration is 20.

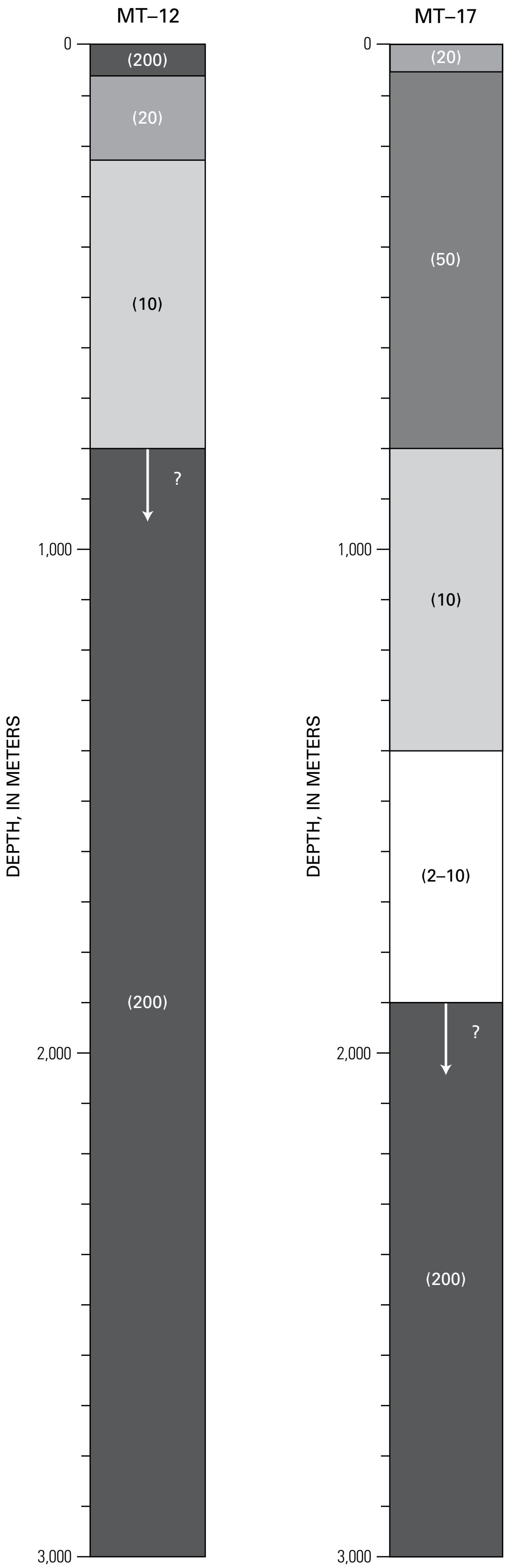

Figure F6. Two-dimensional finite-element resistivity model from low-frequency magnetotelluric (MT) data for MT sounding stations 12 and 17 (see fig. F2*B* for locations). Arrow near question mark within the model indicates uncertainty in placement of boundary.

the upper part of the Santa Fe Group. This conductive interval is underlain by moderately conductive rocks (10 ohm-m); those rocks, which probably include a saturated, fine-grained Santa Fe interval, volcaniclastic Oligocene Espinaso Formation, and possibly the Eocene Galisteo Formation sedimentary rocks, have a composite thickness of 100±20 m. Some part of the weathered Mancos Shale could be included within this 10-ohm-m zone below the basalt. However, the very conductive horizon (2 ohm-m) beginning at a depth of 180±20 m below the AMT station is likely clay-rich Cretaceous marine deposits of the Mancos Shale. Preliminary MT models of this sounding show that the conductive interval is 620±80 m thick. Beneath this very conductive interval, less conductive rocks (5 ohm-m) probably include units of Permian, Triassic, and Jurassic sedimentary rocks.

A resistive interval of basalts (1,000 ohm-m) of the Cerros del Rio at station 5 (fig. F4*A*) are 250±25 m thick. This basalt interval ranges from 60 to 250 m thick between stations 4 and 5. Approximately 140 m of the 250 m basalt thickness at station 5 reflects constructional topography resulting from the growth of basaltic volcanoes. A remarkably detailed driller's log (fig. F4*B*) exists for a water well (the 1200-Foot well) 200 m northwest of AMT station 5. The thickness of the basalt (256 m) measured on a lithology log constructed from the driller's record corresponds closely with the thickness of basalt determined in the AMT model (250±25 m). As recorded in the driller's log, the static water elevation lay at 307 m depth, so our forward modeling used a value of 100 ohm-m for the unsaturated Santa Fe Group sand and gravel above the water table. Saturated sand and silty sand of the Santa Fe Group typically have resistivities in the 20–70 ohm-m range. The modeled electrical sounding shows that 20 ohm-m material extends to a depth of 900±100 m. Beneath the 20 ohm-m material is a 10 ohm-m interval with a thickness of 250±100 m. The 10 ohm-m material may include early Tertiary Galisteo and Espinaso Formations that cannot be separated from Santa Fe Group solely on the basis of their electrical signatures. Espinaso Formation is found in the Yates La Mesa petroleum test well 2 (10 km to the northeast, north of the Santa Fe River, pl. 2), but deposits of the Galisteo may have been eroded or never deposited to the north. Very conductive (2 ohm-m) inferred Mancos Shale occurs at a depth of 1,150±100 m and has lower electrical resistivity than other units in the region. Between station 4, where the top of the Mancos is 1,700 m above sea level, and station 5, where it is 900 m, the top of the Mancos apparently drops 800 m. Thus, these MT results provide evidence for 800 m of Tertiary structural relief at the north end of the Cerrillos uplift. The shallow Mancos Shale located at AMT station 4, immediately south of Tetilla Peak, provides the

Table F2. Range of average resistivity values in regional induction logs for stratigraphic units intersected in wells in study region.

[Well abbreviations: B, Black Oil Ferrill 5; C, CEPO 2; D, Dome Road; PB, Pelto Blackshare 1; PO, Pelto Ortiz 1; T, Transocean McKee 1; S, Shell Laguna Wilson Trust 1]

Epoch or Period	Stratigraphic unit or level	Ohm-m	Thickness (m)	Well
Pliocene–Miocene	Santa Fe Group	8–70	400–451	D, PB, C
Oligocene	Espinaso Formation	10–20	533	PB
Eocene	Galisteo Formation	5–20	526–1,376	PB, PO, B
Cretaceous	Upper	2–40	420–1,526	PB, PO, B, S, T
Jurassic	Upper/Middle	2–20	223–453	PB, S, T
Triassic	Upper	2–15	482–933	S, T
Permian	Upper/Lower	6–200	262–659	S, T
Pennsylvanian	Upper/Middle/Lower	7–200	585–766	S, T

Table F3. Location of wells referred to in table F2.

[Coordinates listed below are referenced to the 1866 Clarke spheroid and North American 1927 datum; stations listed in order from west to east; locations determined using a global positioning system; longitude and latitude format is decimal degrees; UTM, Universal Transverse Mercator]

Well	Longitude	Latitude	UTM (m)		Elevation	
			North	East	(m)	(ft)
B	–106.041	35.386	3,916,149	13,405,451	1,787	5,889
C	–106.351	35.627	3,943,183	13,377,650	1,632	5,379
D	–106.365	35.683	3,949,468	13,376,462	1,765	5,818
PB	–106.269	35.397	3,917,611	13,384,758	1,831	6,034
PO	–106.058	35.412	3,919,049	13,403,938	1,761	5,804
T	–105.990	35.390	3,916,545	13,410,088	1,801	5,935
S	–106.968	35.024	3,877,277	13,320,453	1,643	5,415

farthest northwest constraint for the edge of the Cerrillos uplift. This AMT-defined northwest edge is consistent with the subsurface extent of the uplift on the basis of gravity data (chapter D, this volume). The feeder dike shown in figure F4*A* may be oriented in any one of several azimuthal directions with respect to station 5. It could correspond with dikes associated with the Cerro Colorado vent to the west (fig. F7*A*), the Cerrito Portrillo andesite volcano to the northeast (pl. 2), or a N. 20° E.–trending linear chain of younger basalts and andesites to the southeast (pl. 2). The high accuracy of the thickness of resistive basalt determined by the sounding at AMT station 5, as compared with the driller's log for the 1200-Foot well, suggests that electrical soundings of this type may be an accurate method of determining the thickness of volcanic deposits in the Cerros del Rio volcanic field and in similar settings underlain by shallow volcanic rocks of variable thickness. The advantage of the ground AMT soundings is the much greater depth of investigation, as much as 1,200 m in the AMT station 5 example, as opposed to a maximum depth of about 300 m depth for the airborne TDEM data in a favorable situation (for example, no thick, shallow conductors). Detailed comparison of the AMT data from station 5 with the lithologic log from the 1200-Foot well (fig. F4*B*) also provides some insight into the degree of resolution of the AMT soundings and plan-mapping techniques: Modeling of the AMT data was able to resolve the thickness of resistive basalt only to within 10 percent. Also, in the upper 47 m, we were not able to distinguish the 24-m interval of dry basalt cinders from

Figure F7 (facing and following 5 pages). Depth slices in the Cochiti Pueblo time-domain electromagnetic survey area (*A*–*F*), drawn on the basis of least-squares inversions. Solid numbered triangles represent high-frequency magnetotelluric sounding stations. C3, C4, C5, W4, magnetic anomalies discussed in chapter D (this volume); F, inferred fine grain size sediments; V, inferred volcanic rock. *A*, 20-m-depth slice. *B*, 50-m-depth slice. *C*, 70-m-depth slice. *D*, 100-m-depth slice. *E*, 150-m-depth slice. *F*, 200-m-depth slice.

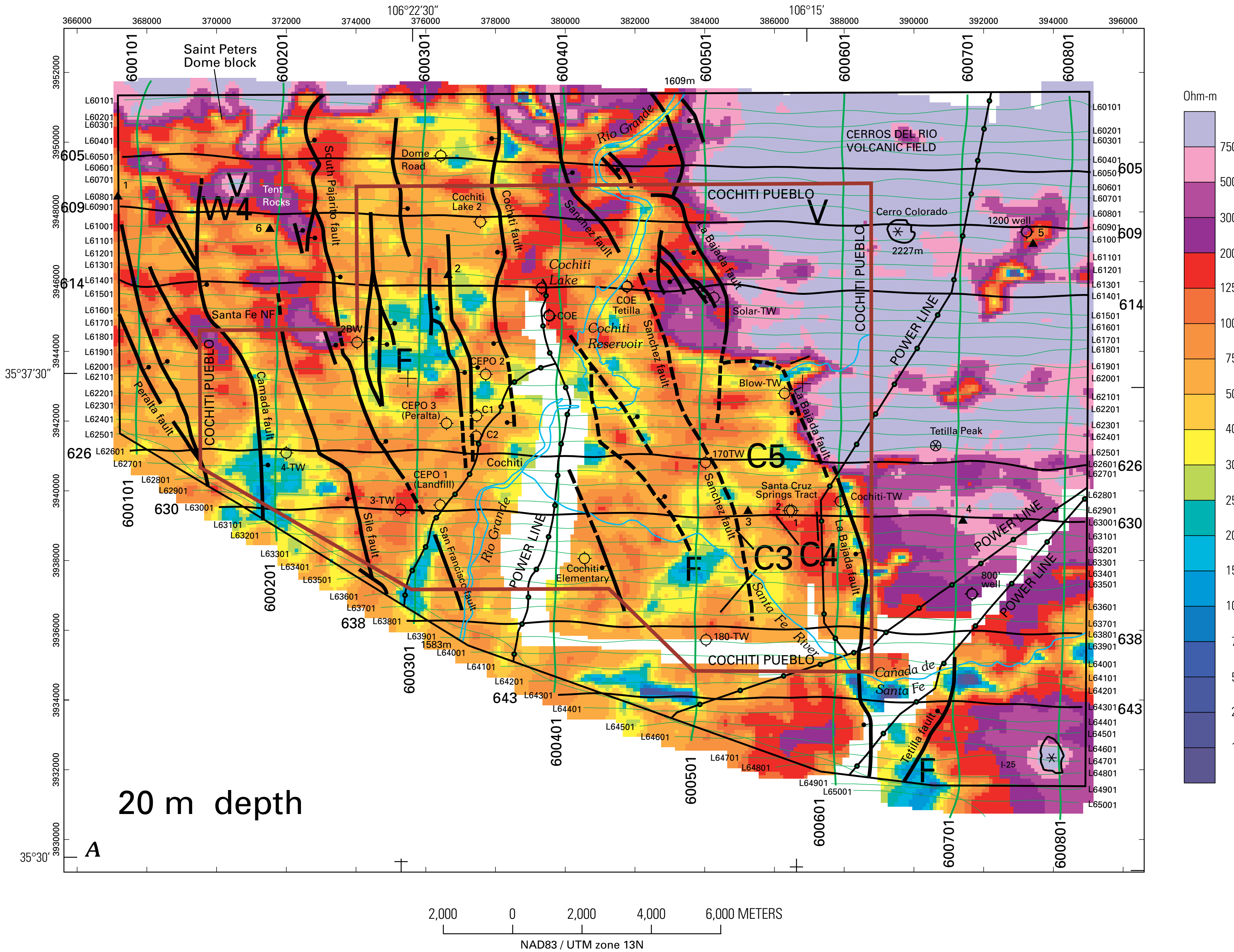

20 m depth
A
Ohm-m
750.0
500.0
300.0
200.0
125.0
100.0
75.0
50.0
40.0
30.0
25.0
20.0
15.0
10.0
7.5
5.0
2.5
1.0
COCHITI PUEBLO
CERROS DEL RIO VOLCANIC FIELD
Saint Peters Dome block
Cochiti Lake
Cochiti Reservoir
Rio Grande
Santa Fe River
Cañada de Santa Fe
POWER LINE
2,000 0 2,000 4,000 6,000 METERS
NAD83 / UTM zone 13N

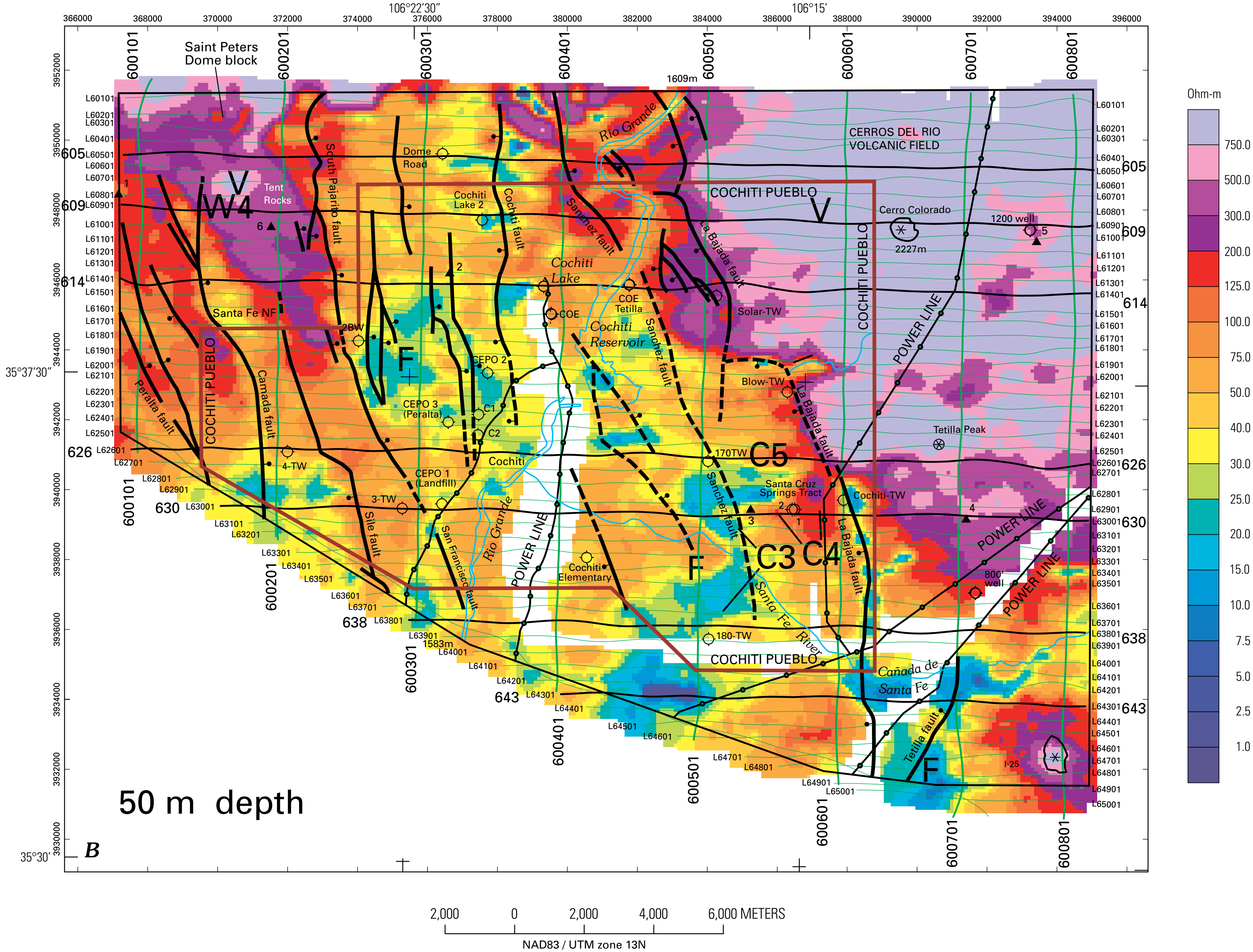

50 m depth
B
Ohm-m
750.0
500.0
300.0
200.0
125.0
100.0
75.0
50.0
40.0
30.0
25.0
20.0
15.0
10.0
7.5
5.0
2.5
1.0
106°22'30"
106°15'
35°37'30"
35°30'
Saint Peters Dome block
Tent Rocks
CERROS DEL RIO VOLCANIC FIELD
COCHITI PUEBLO
Cerro Colorado
2227m
1200 well
1609m
Dome Road
Cochiti Lake 2
Cochiti Lake
COE Tetilla
COE
Cochiti Reservoir
Solar-TW
Blow-TW
Santa Fe NF
2BW
CEPO 2
CEPO 3 (Peralta)
C1
C2
Cochiti
CEPO 1 (Landfill)
3-TW
4-TW
170TW
Santa Cruz Springs Tract
Cochiti-TW
Cochiti Elementary
180-TW
800' well
Tetilla Peak
1583m
I-25
Rio Grande
Santa Fe River
Cañada de Santa Fe
POWER LINE
South Pajarito fault
Cochiti fault
Sanchez fault
La Bajada fault
Peralta fault
Camada fault
Sile fault
San Francisco fault
Tetilla fault
V
W4
F
C3
C4
C5
605
609
614
626
630
638
643
2,000 0 2,000 4,000 6,000 METERS
NAD83 / UTM zone 13N

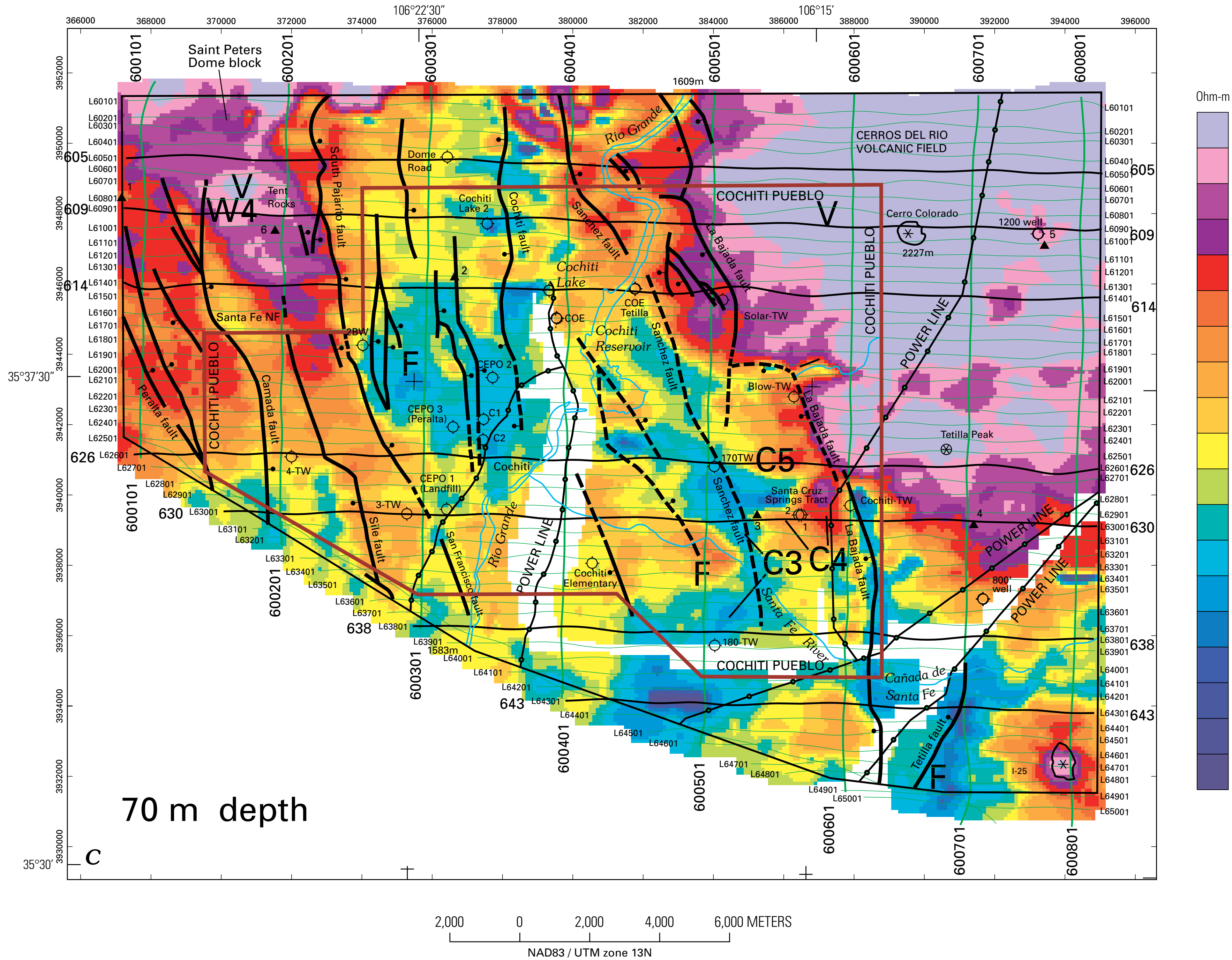
Ohm-m
750.0
500.0
300.0
200.0
125.0
100.0
75.0
50.0
40.0
30.0
25.0
20.0
15.0
10.0
7.5
5.0
2.5
1.0
106°22'30"
106°15'
35°37'30"
35°30'
Saint Peters Dome block
CERROS DEL RIO VOLCANIC FIELD
COCHITI PUEBLO
Cerro Colorado
2227m
1200 well
1609m
Tent Rocks
Dome Road
Cochiti Lake 2
Cochiti Lake
Cochiti Reservoir
Rio Grande
COE
COE Tetilla
Solar-TW
Santa Fe NF
2BW
CEPO 2
CEPO 3 (Peralta)
CEPO 1 (Landfill)
C1
C2
Cochiti
Blow-TW
Tetilla Peak
170TW
Santa Cruz Springs Tract
Cochiti-TW
3-TW
4-TW
Cochiti Elementary
800' well
180-TW
1583m
Cañada de Santa Fe
Santa Fe River
I-25
POWER LINE
South Pajarito fault
Cochiti fault
Sanchez fault
La Bajada fault
Peralta fault
Camada fault
Sile fault
San Francisco fault
Tetilla fault
V
W4
F
C3
C4
C5
70 m depth
c
2,000 0 2,000 4,000 6,000 METERS
NAD83 / UTM zone 13N

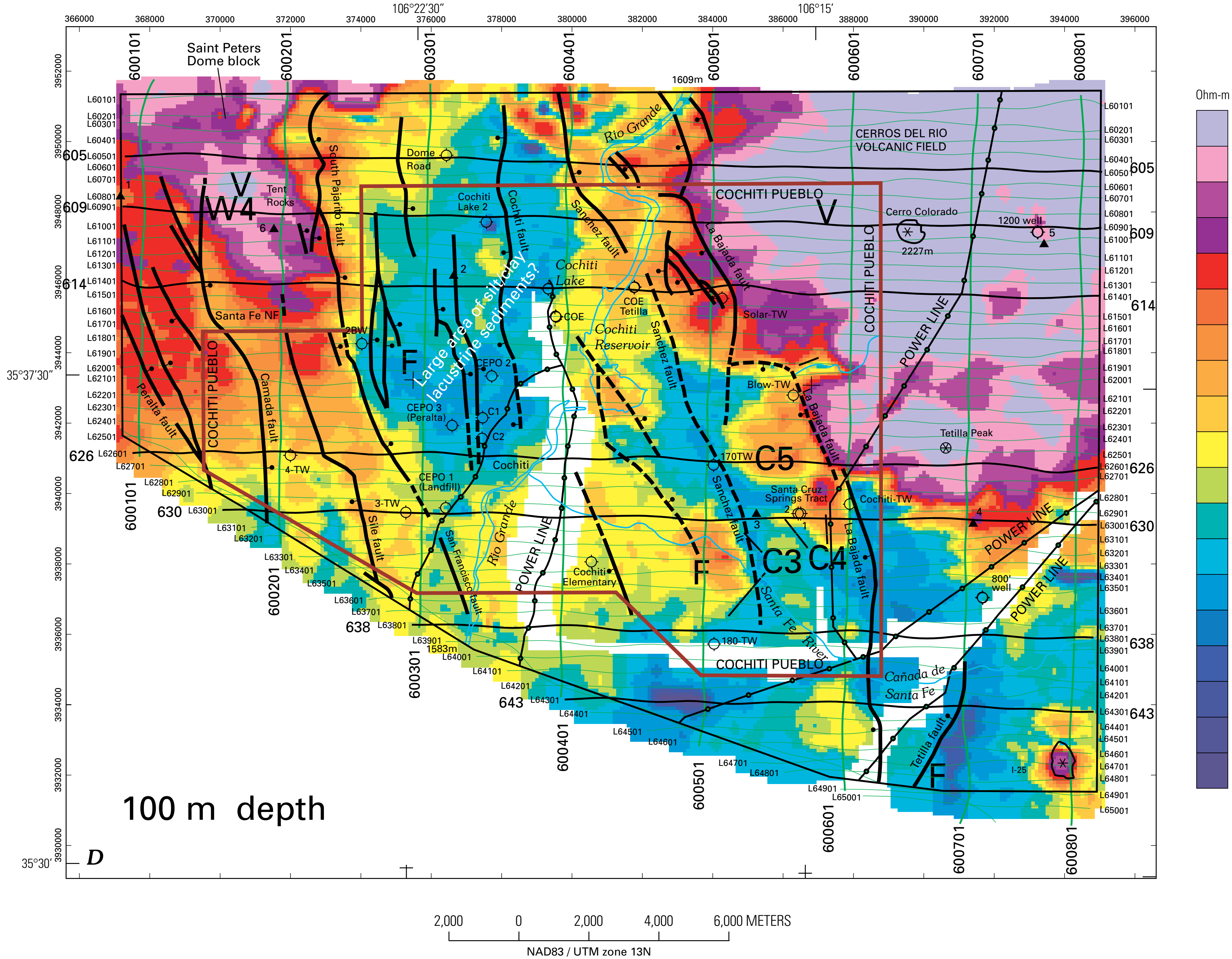
Ohm-m
750.0
500.0
300.0
200.0
125.0
100.0
75.0
50.0
40.0
30.0
25.0
20.0
15.0
10.0
7.5
5.0
2.5
1.0
106°22'30"
106°15'
35°37'30"
35°30'
Saint Peters Dome block
Tent Rocks
W4
V
South Pajarito fault
Dome Road
Cochiti Lake 2
Cochiti fault
Sanchez fault
Rio Grande
1609m
COCHITI PUEBLO
CERROS DEL RIO VOLCANIC FIELD
Cerro Colorado
2227m
1200 well
La Bajada fault
Cochiti Lake
COE
COE Tetilla
Cochiti Reservoir
Large area of silt/clay lacustrine sediments?
Solar-TW
POWER LINE
Santa Fe NF
2BW
F
CEPO 2
CEPO 3 (Peralta)
C1
C2
Blow-TW
Tetilla Peak
Peralta fault
Camada fault
4-TW
Cochiti
CEPO 1 (Landfill)
170TW
C5
Santa Cruz Springs Tract
Cochiti-TW
3-TW
Sile fault
San Francisco fault
Cochiti Elementary
C3
C4
800' well
Santa Fe River
180-TW
Cañada de Santa Fe
Tetilla fault
1583m
I-25
100 m depth
D
2,000 0 2,000 4,000 6,000 METERS
NAD83 / UTM zone 13N

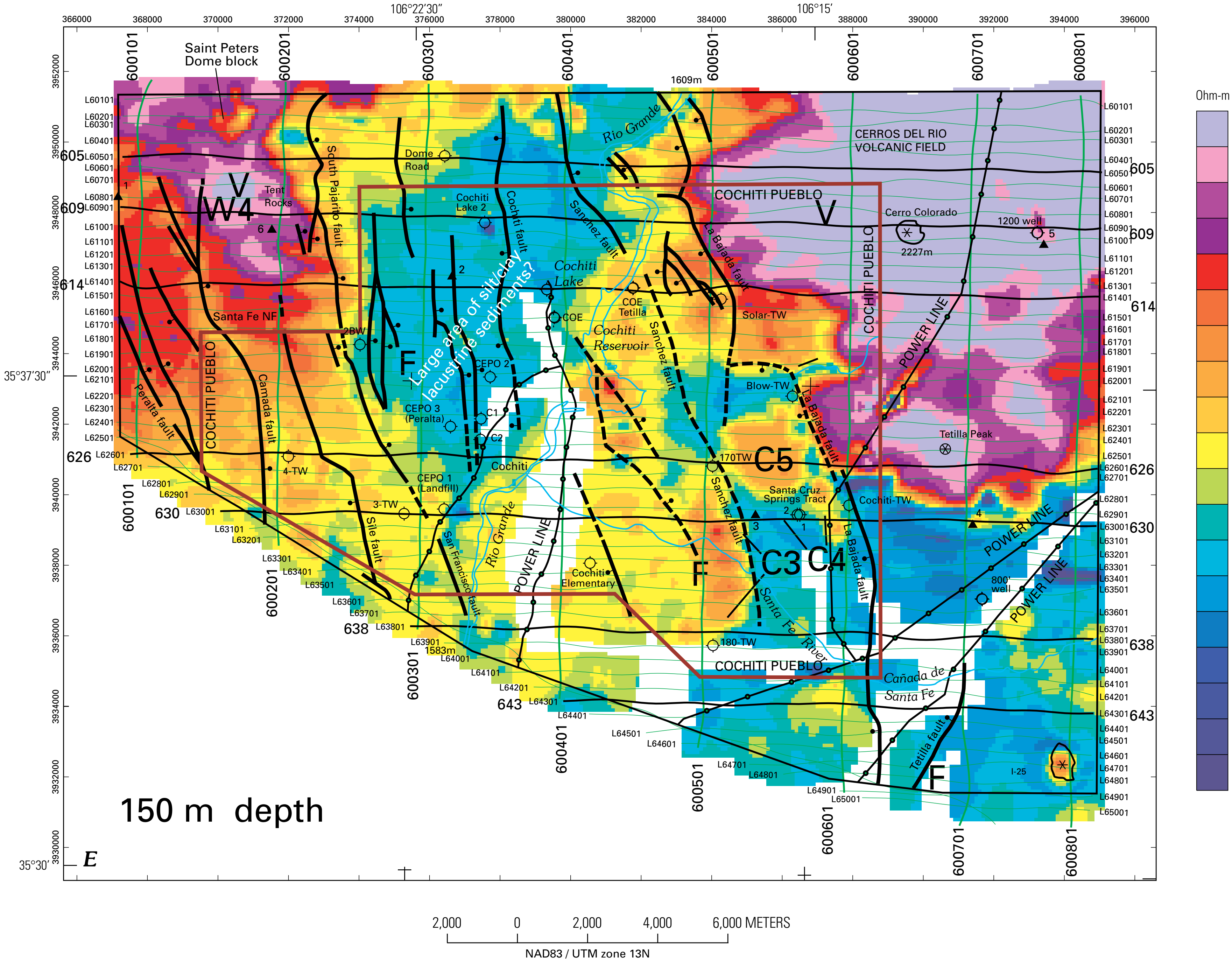

150 m depth
E
Ohm-m
750.0
500.0
300.0
200.0
125.0
100.0
75.0
50.0
40.0
30.0
25.0
20.0
15.0
10.0
7.5
5.0
2.5
1.0
106°22'30"
106°15'
35°37'30"
35°30'
Saint Peters Dome block
CERROS DEL RIO VOLCANIC FIELD
COCHITI PUEBLO
Cerro Colorado
2227m
1200 well
1609m
Rio Grande
Dome Road
Tent Rocks
Cochiti Lake 2
Cochiti fault
Sanchez fault
La Bajada fault
South Pajarito fault
Cochiti Lake
Large area of silt/clay lacustrine sediments?
COE
COE Tetilla
Cochiti Reservoir
Solar-TW
Santa Fe NF
2BW
CEPO 2
CEPO 3 (Peralta)
C1
C2
Blow-TW
Tetilla Peak
Peralta fault
Camada fault
4-TW
170TW
C5
Cochiti
CEPO 1 (Landfill)
3-TW
Sile fault
San Francisco fault
POWER LINE
Santa Cruz Springs Tract
Cochiti-TW
Cochiti Elementary
C3
C4
F
V
W4
800' well
Santa Fe River
180-TW
Cañada de Santa Fe
Tetilla fault
I-25
1583m
2,000 0 2,000 4,000 6,000 METERS
NAD83 / UTM zone 13N

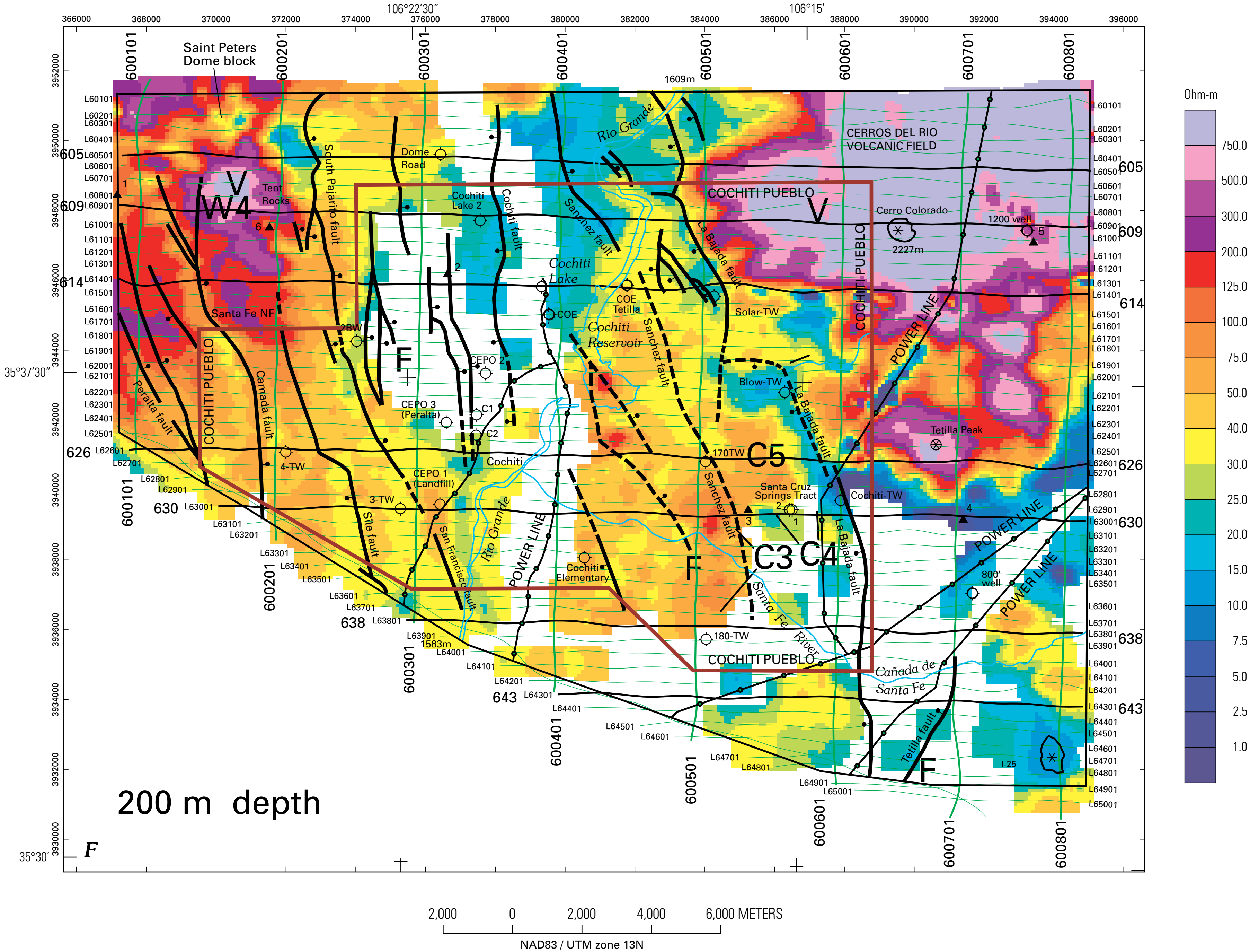

106°22'30"
106°15'
35°37'30"
35°30'
Saint Peters Dome block
Tent Rocks
W4
V
Santa Fe NF
COCHITI PUEBLO
Peralta fault
Camada fault
South Pajarito fault
Sile fault
San Francisco fault
Cochiti fault
Sanchez fault
La Bajada fault
Tetilla fault
Dome Road
Cochiti Lake 2
Cochiti Lake
COE
COE Tetilla
Cochiti Reservoir
2BW
CEPO 2
CEPO 3 (Peralta)
CEPO 1 (Landfill)
C1
C2
Cochiti
4-TW
3-TW
Cochiti Elementary
Rio Grande
POWER LINE
1609m
1583m
Solar-TW
Blow-TW
170TW
C5
C3
C4
Santa Cruz Springs Tract
Cochiti-TW
180-TW
Santa Fe River
Cañada de Santa Fe
CERROS DEL RIO VOLCANIC FIELD
Cerro Colorado
2227m
1200 well
Tetilla Peak
800' well
I-25
F
200 m depth
Ohm-m
750.0
500.0
300.0
200.0
125.0
100.0
75.0
50.0
40.0
30.0
25.0
20.0
15.0
10.0
7.5
5.0
2.5
1.0
2,000 0 2,000 4,000 6,000 METERS
NAD83 / UTM zone 13N

hard basalt beneath, because the resistivity of the cinders was intermediate between the resistivities of the dry clay and the hard basalt.

The northwest-southeast profile, A-A′ (fig. F2*A*) in the Cochiti Pueblo area is based on four AMT stations. The profile extends across the South Pajarito fault (fig. F5). The westernmost sounding (station 1) was made in the Saint Peters Dome block; the three eastern soundings on the profile (stations 6, 2, and 3) were made in the northeast part of the Santo Domingo Basin. At stations 1 and 6, volcanic rocks and interstratified volcaniclastic deposits are at the surface and in the upper part of the profile. Station 1 is just outside (to the west) of the area of the geologic map compilation of the Cochiti Pueblo area shown in plate 2. The geology under station 1 consists of thin Pliocene gravel of Lookout Park overlying Cochiti Formation in the footwall block of the Camada fault. On the basis of aeromagnetic and TDEM data, it appears that station 1 is just outside the area of Miocene Bearhead Rhyolite lava domes and intrusions and the shallow deposits consist of very proximal coarse, high-resistivity volcaniclastic Cochiti Formation (100 ohm-m) from 2,060 m to about 1,940 m elevation. This material is underlain by a 150±30-m-thick interval of moderate resistivity (30 ohm-m) that probably correlates with medium-grained sand and gravel of the Cochiti Formation. The bottom of the profile has low resistivity (10 ohm-m) and probably is silt and silty fine sand within the Cochiti Formation or possibly even middle Miocene deposits of the Santa Fe Group that are locally present in the Saint Peters Dome block beneath upper Miocene Keres Group basalt, andesite, and rhyolite volcanic rocks. The base of the 10 ohm-m material is not resolved by the AMT sounding, but it has a minimum thickness of 310±60 m.

AMT station 6 is located in Peralta Canyon within the Kashe-Katuwe Tent Rocks National Monument (pl. 1) in thin Quaternary alluvium directly adjoining large cliff exposures of Peralta Tuff Member of the Bearhead Rhyolite and overlying basal Cochiti Formation (pl. 2). The upper 30 m of AMT sounding 6 consists of high-resistivity (300 ohm-m) (fig. F5) rhyolite lava and coarse proximal breccia or sediments derived from the extrusive dome of Bearhead Rhyolite exposed in lower Peralta Canyon (Smith, 2001). The underlying 150 m of moderately resistive material (100 ohm-m) may be coarse-grained sedimentary material derived from the Bearhead Rhyolite, or it may be similar near-vent breccias and pyroclastic deposits partially to wholly saturated by a perched water table. These volcanic or volcaniclastic materials are underlain by moderately conductive saturated, coarse-grained deposits (30 ohm-m) of the Santa Fe Group (Cochiti Formation) that have a thickness of 220±40 m. Beneath it is a more conductive saturated fine-grained sedimentary interval (10 ohm-m), probably in the middle part of the Santa Fe Group, whose base was not resolved but which has a minimum thickness of 600±100 m. The similar sequences of resistivities between stations 1 and 6 argue for considerable eastward thickening of the more resistive 100 ohm-m and 30 ohm-m intervals across the Camada fault and for similar thickening of fine-grained Santa Fe Group(?) sediments (10 ohm-m) beneath them.

AMT stations 2 and 3, in the northeast part of the Santo Domingo Basin, reflect electrical responses of basin-fill sediments of the Santa Fe Group. A moderately conductive, unsaturated, fine-grained Santa Fe interval (30 ohm-m), and the lower part of the Bandelier Tuff (Otowi Member) immediately beneath station 2 (fig. F5) have a combined thickness of 60±10 m. A conductive fine-grained Santa Fe sedimentary interval (10 ohm-m) beneath has a minimum thickness of 360±40 m. Although relatively coarse grained Cochiti Formation is widespread on the west side of the Rio Grande, at AMT sounding 2 we did not resolve a moderate- to high-resistivity unit below the water table. We cannot determine from the AMT data the electrical characteristics beneath this thick conductive interval. Such are the limitations of sparse data sampled more than a kilometer apart. Nevertheless, nearby subsurface deposits of the ancient Rio Grande should be widespread. The shallow part of the conductor at AMT station 2, at depths of 60–200 m or more, may be a different fine-grained Santa Fe facies. The well log from CEPO 2 (fig. F8*B*) shows a prominent conductor of less than 10 ohm-m at 160–260 ft (49–79 m) depth.

At AMT station 3 (fig. F5), east of the Rio Grande, a resistive, unsaturated, medium-grained Santa Fe interval (100 ohm-m) is 45±5 m thick. A resistive inferred basaltic vent (100 ohm-m) at 140±20 m depth has a minimum thickness of 860±100 m and is offset relative to the vertical sounding. Underlying, moderately conductive, saturated Santa Fe Group sediments (30 ohm-m) are likely medium to coarse (axial) sand and lesser gravel with a minimum thickness of 550±60 m. A more conductive fine-grained Santa Fe interval (10 ohm-m) beneath has a minimum thickness of 100±50 m. An underlying very conductive interval (2 ohm-m), at an elevation of 960 m, may be Mancos Shale. If so, the elevation of the top of the Mancos Shale drops 760 m between station 3 (fig. F5) and station 4 (fig. F4*A*) across the La Bajada fault zone (fig. F2*A*).

MT station 12 is located west of Saint Peters Dome to the north of the area of the geologic map of the Cochiti Pueblo area (pl. 2, fig. F2*B*). Upper resistive material (200 ohm-m) directly beneath station 12 (fig. F6) has a thickness of 60±10 m. Bandelier Tuff is exposed nearby at the surface. Moderately conductive material (20 ohm-m) beneath, which has a minimum thickness of 165±20 m, is probably a medium-grained sedimentary facies of the Santa Fe Group. A more conductive interval (10 ohm-m) below probably includes fine-grained Santa Fe Group sediments, Espinaso Formation volcaniclastic rocks, and Galisteo Formation sedimentary rocks that have a composite minimum thickness of 575±100 m. Poor data quality prevented us from solving for its maximum thickness. We modeled resistive material (200 ohm-m) at a minimum depth of 800±100 m that may be Paleozoic limestones. The top of this resistive interval is about 1,580 m above sea level. Because of poor data quality and the three-dimensional MT response at low frequencies, we are less certain of its true elevation and resistivity.

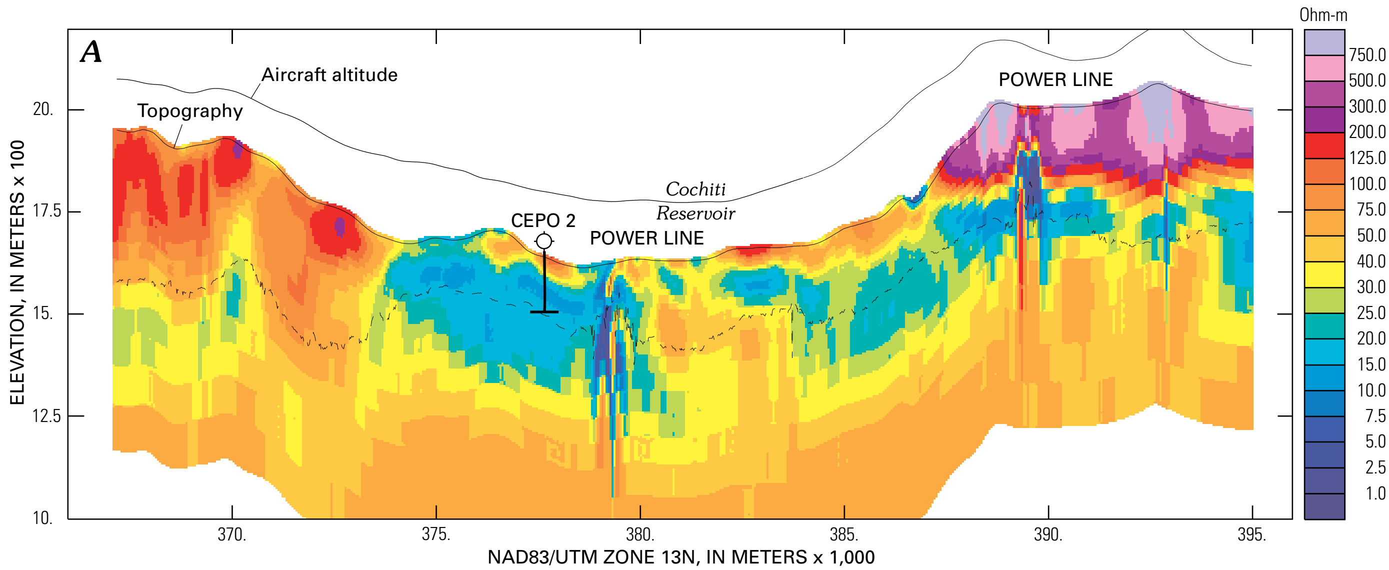

Figure F8 (above and facing page). *A*, Resistivity under flight line 620 in the Cochiti Pueblo time-domain electromagnetic survey area, drawn on the basis of least-squares inversion and showing location of CEPO 2 induction-resistivity well. Line floating above cross section represents aircraft altitude; faint dashed line represents maximum valid depth limit used for geologic interpretations. Vertical exaggeration is 10. *B*, Induction-resistivity log for well CEPO 2 in Cochiti Pueblo. Solid line is long-normal (induction) resistivity; faint dashed line is 30-ft moving average of long-normal resistivity; open circles connected with black dashed line indicate depths of resistivity contours (15, 20, 25, 30, 40, 50, 75, 100, and 125 ohm-m values) obtained from resistivity inversion shown in figure F8*A*; SWL is static water level. Grain size labels (Coarse, Medium, Fine) refer to bulk average lithology of the middle Rio Grande Basin Santa Fe Group sediments (Cole and others, 1999). Lithologic descriptions to left of grain-size labels from figure G4.

MT station 17 is located near the Dome Road well (fig. F2*A*) in the La Bajada constriction. The 400 m of section within the Dome Road well consists almost entirely of Cochiti Formation sand and gravel (Chamberlin, Jackson, and Connell, 1999). An induction-resistivity log (fig. G5) shows average resistivities that range from about 20 ohm-m to 60 ohm-m and a median resistivity of about 40 ohm-m. An uppermost, moderately conductive (20 ohm-m), 50±10-m-thick interval at MT station 17 (fig. F6) correlates with the 30 ohm-m average resistivity logged in the upper 70 m of the Dome Road well. An underlying, moderately resistive (50 ohm-m) interval, 750±80 m thick, correlates with the induction log resistivities that averaged 30 ohm-m between depths of 70–250 m and with average resistivities that ranged from 30 to 60 ohm-m at depths of 250–400 m (the base of the log). Moderately conductive material (10 ohm-m) below probably includes fine-grained sediments of the Cochiti Formation, volcaniclastic sedimentary rocks of the Espinaso Formation, and Galisteo Formation sedimentary rocks that have a composite thickness of 600±100 m. Beneath this interval is a conductive section (2–10 ohm-m) that may contain carbonaceous shale of the Cretaceous Menefee Formation and Mancos Shale, Jurassic sandstones, and mudstones of the Triassic Chinle Formation. The elevation of the top of this interval is about 350 m above sea level, which represents a drop in elevation of 610 m relative to a similar interval at station 3. If the conductive intervals beneath stations 17 and 3 represent the same geologic horizons, then the resistivity structure beneath station 17 reveals a deepening of the Rio Grande rift. We modeled resistive material (200 ohm-m) at a minimum depth of 1,900±150 m (–150 m elevation) at station 17 that may be Paleozoic limestone. As we stated at the beginning of this section, these geologic interpretations were guided by induction log resistivities from several wells in the region (tables F2, F3). If these inferred geologic horizons are correct, then the boundary between the 2–10 ohm-m and the 200 ohm-m layers represents the boundary between Mesozoic and Paleozoic rocks. Thus, these MT results have provided additional constraints on the relative positions of basement rocks and the thicknesses of Paleozoic, Mesozoic, and Tertiary sedimentary rocks on either side of the Pajarito fault zone.

Airborne Electromagnetic Surveys

The airborne time-domain electromagnetic (TDEM) method is an active geophysical technique that uses artificially generated electromagnetic fields to investigate the electrical resistivity of the subsurface. The TDEM method probes the electrical properties of the Earth from depths of a few meters to depths of several hundred meters depending on the geology and the TDEM system specifications. The depth of investigation can reach hundreds of meters in cases of very resistive, dry, low-porosity rocks such as unweathered volcanic rocks but only about 100 m in water-saturated clay-rich sediments that are markedly less resistive than unweathered volcanic rocks.

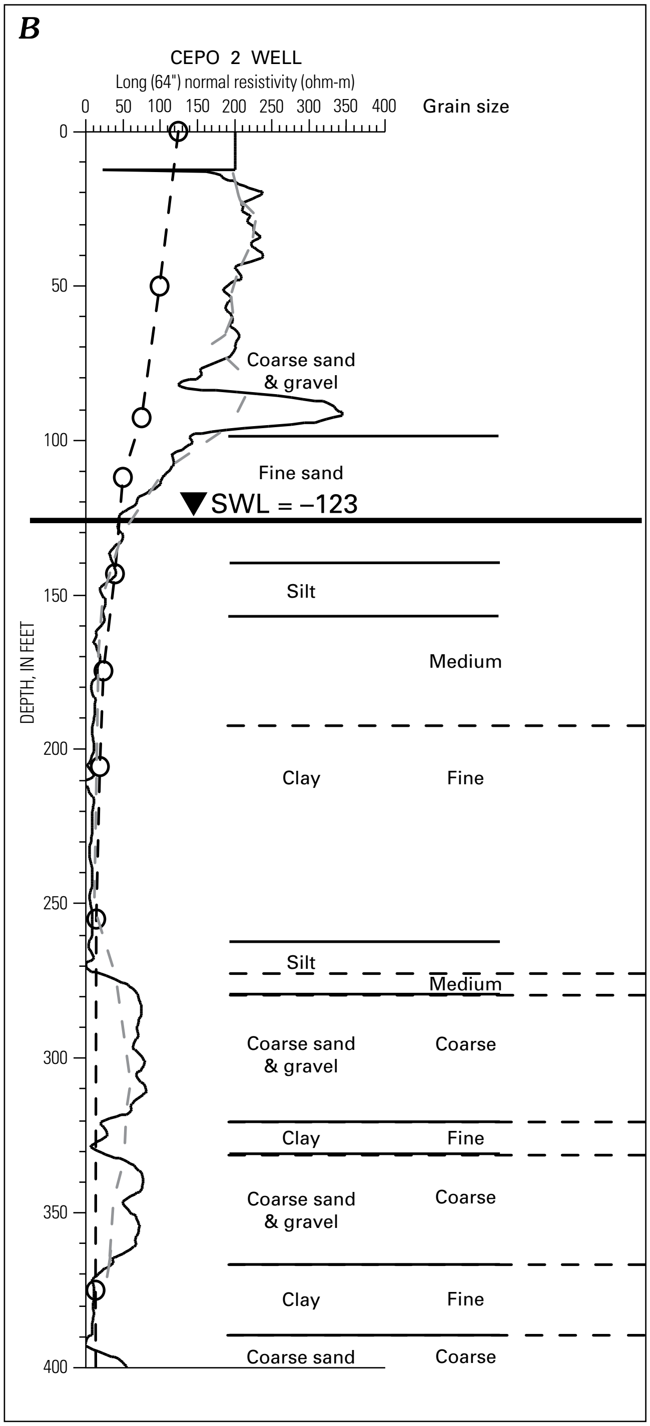

Furthermore, the resistivity of the upper few meters may not be well resolved in the case of conductive near-surface rocks, and the upper tens of meters may not be well resolved in the case of resistive rocks. The depth of penetration and the resolution of the model can be modified by the choice of TDEM system and by incorporating survey parameters designed to target a particular geologic problem.

In a typical TDEM system, a loop of current-carrying wire (the transmitter) is mounted on an aircraft and sends pulses of electromagnetic energy (usually 30–90 times per second) at fixed time intervals. A receiver is mounted in a cigar-shaped unit, commonly called a bird, that is towed on a cable below and behind the aircraft. The receiver measures the electromagnetic impulses as a function of time. The shape of the impulses measured by the receiver and their decay rates after the cessation of the transmitter current are affected by the presence of the Earth. In general (assuming that all system and survey parameters remain constant), a stronger signal and slower rate of decay indicate lower resistivity in the subsurface, whereas a weaker signal and faster rate of decay indicate higher resistivity. Signals recorded at earlier times (microseconds after current turnoff) provide information on shallower depths, whereas signals recorded at later times (milliseconds after current turnoff) provide information on deeper depths (Palacky and West, 1991). Lower rates at which transmitted pulses are repeated allow longer measurements of signal decay between pulses; resistivity information is thus obtained from deeper subsurface regions. The tradeoff for deeper penetration is lower horizontal resolution along the flight lines. The horizontal resolution also depends on the TDEM system dimensions and the survey parameters such as flight elevation and flight-line spacing. The signal received is affected by many factors, but ideally the strength of the signal recorded at a given time reflects the resistivity distribution in the subsurface. The measured voltages can be modeled as electrical resistivity distribution with depth.

Several factors dictated the decision to use the airborne TDEM method for this investigation. First, airborne methods efficiently collect large amounts of information over a wide area. Spatial sampling of the subsurface is determined by the line spacing and by the sampling rate along the flight lines. Second, airborne TDEM can be used to infer the general distribution of electrical resistivity to depths greater than is typically possible in frequency-domain airborne electromagnetic surveys. Third, the method can be applied in difficult terrain that is not readily accessible by road for ground-based electromagnetic methods. Access was a controlling factor for much of the survey area, because of sparse roads in and around Cochiti Pueblo.

One drawback of the method is that cultural features, because of their wide bandwidth, strongly affect the responses of the TDEM system. Fences, pipelines, communication lines, railways, and other man-made conductors can contaminate the responses. The areas affected by such cultural noise cannot be used for interpretation. The majority of cultural anomalies can be easily identified, but sometimes the cultural noise response is subtle and can be mistaken for the Earth's response. Cultural noise in this survey severely affected only a very limited part of the TDEM data, mainly near a few large power lines (fig. F2*A*).

Time-Domain Electromagnetic Survey

Airborne TDEM data were collected on March 3–7, 1997, by Geoterrex, Inc., which used a GEOTEM system (Deszcz-Pan and others, 2000). The survey area is in the vicinity of Cochiti

Pueblo (pl. 1; survey area D, fig. F1). The purpose of the survey was to delineate facies changes within the basin fill that may control local and regional ground-water flow and to help define the three-dimensional extent of the principal axial-river gravel aquifer in the subsurface of the Santa Fe Group basin fill. In the GEOTEM system, a transmitter mounted on an airplane pulses an electromagnetic signal 30 times per second. In the receiver, towed about 50 m below and 125 m behind the airplane, the electromagnetic signal is recorded as a voltage at specific times during and after each pulse.

The receiver measures three spatial components of the transmitter signal: x, y, and z. Our interpretations are based primarily on the z-component (vertical) of the received signal. The x-component (in-line) was processed but was used only to check consistency between the x- and z-components. The y-component (transverse) was ignored because this component should be zero in the one-dimensional geometry that was assumed for the processing of the data.

The Cochiti Pueblo survey covered approximately a 15×20 km area. The aircraft was flown at 120 m above ground level using a 400-m flight-line spacing (fig. F2*A*). Above the small urban area in the Cochiti Pueblo, the flight height reached about 250 m above ground level. During the five days of the Cochiti survey, about 100,000 soundings were recorded. The sounding spacing along the flight lines was about 13 m. At each of the sounding points, 60 channels of time-domain data were recorded, 20 in each of the x, y, and z spatial directions. Of the 20 channels, 4 channels recorded a signal when the transmitter pulse was on, and 16 channels were designated to record the signal received after the transmitter signal ended. The transmitter signal was a half-sinusoidal wave that was on for 4.166 ms and off for 13.371 ms.

Resistivity Models Based on Time-Domain Electromagnetic Survey

Inversion of recorded signal to resistivities does not produce a single, unique result; the result depends on the algorithms used. All algorithms are based on the assumption that the calculated response from a given Earth model must match the measured fields within some specified error. All models are approximations and not a true resistivity distribution in the Earth. In the inversion of this TDEM data we assumed a one-dimensional model such that under each survey point the resistivity changes only in one dimension: depth. By stitching together the resistivity models for each point along the flight lines we obtained a resistivity cross section along each flight line. Maps of resistivity at given depths below the surface, or at given elevations above sea level, were obtained by combining resistivity cross sections from the flight lines.

Inversion results for the survey were provided courtesy of BHP World Minerals. Two proprietary one-dimensional Earth resistivity algorithms were used in inverting the TDEM data: one based on a layered Earth model and a second based on a thin-sheet Earth model. In the first model the subsurface is approximated by a stack of horizontal layers, each having a certain resistivity and thickness. In this algorithm (Ellis, 1998), for each survey point, the fields measured at 16 time-channels after the transmitter current turnoff were simultaneously compared with calculated responses. The least-squares error between measured and calculated data was minimized by iteratively adjusting the resistivity model until the error diminished to a specified value. The inversion model consists of 24 layers of fixed thickness over a half-space (thick homogeneous bottom model layer). The layer thicknesses are initially specified and remain constant along the flight line. The layer thicknesses increase from 5 m on the surface to 110 m for the deepest layer in proportion to the decrease in resolution with depth of electromagnetic methods. The basement resistivity was fixed at 50 ohm-m. The depth of this artificial basement (780 m) is well below the signal-penetration depth, but experience shows that the presence of a deep basement of fixed resistivity stabilizes the inversion algorithm. The model calculations are quite complicated and time consuming.

The second model assumes that measured responses at two measurement times can be modeled by a thin, conductive sheet floating in free space. An assembly of sheets whose calculated responses matches the responses measured at two subsequent times, moving from the earliest to the latest, represent subsurface resistivity as a function of increasing depth. In this algorithm (Liu and Asten, 1993) a conductive, horizontal, thin sheet in free space is used to approximate Earth resistivity distribution with depth. The measured responses at the two earliest times after the transmitter current is turned off are used to uniquely determine conductance and the distance between the thin sheet and the receiver. Then the position and conductance of the sheet matching the responses at the next pair of later times is found. The process is continued for all later pairs. The model resulting from this transformation is called a resistivity depth image (Deszcz-Pan and others, 2000). The calculated response for the thin sheet is analytic so the algebraic transformation calculations are very fast and simple.

Both model algorithms have their merits; however, we found that the layered model resistivities better matched induction log resistivities and MT models. When we compared results obtained by three geophysical methods—resistivity models calculated from AMT soundings, bulk average resistivities calculated from induction logs, and resistivity cross sections calculated by least-squares inversion—we found that the maximum depth provided by the resistivity-depth-image cross sections (for example, fig. F9) could be used as the maximum valid depth limit for the least-squares resistivity inversion. We plotted this maximum depth on each least-squares resistivity inversion cross section at any given point along the flight line. This maximum resistivity-depth-image depth is shown as a dashed line on the inversion cross section (for example, fig. F10). AMT and TDEM models correlate well, as shown by a comparison of AMT soundings and one of the least-squares inversion cross sections (fig. F11*D*). Some exceptions occurred near the maximum resistivity-depth-image depth limit (especially when a conductor at

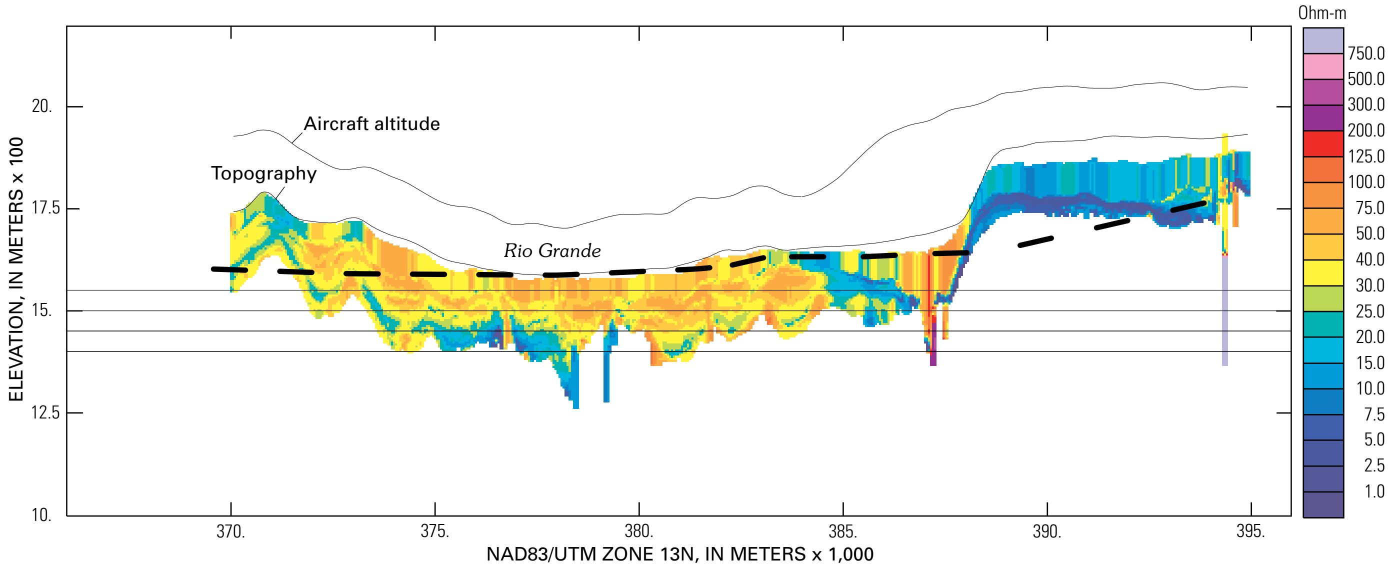

Figure F9. Resistivity under flight line 630 in the Cochiti Pueblo time-domain electromagnetic survey area, drawn on the basis of resistivity-depth image algorithm. Solid horizontal lines represent subsurface elevations 1,400, 1,450, 1,500, and 1,550 m. Line floating above cross section represents aircraft altitude. Vertical exaggeration is 10.

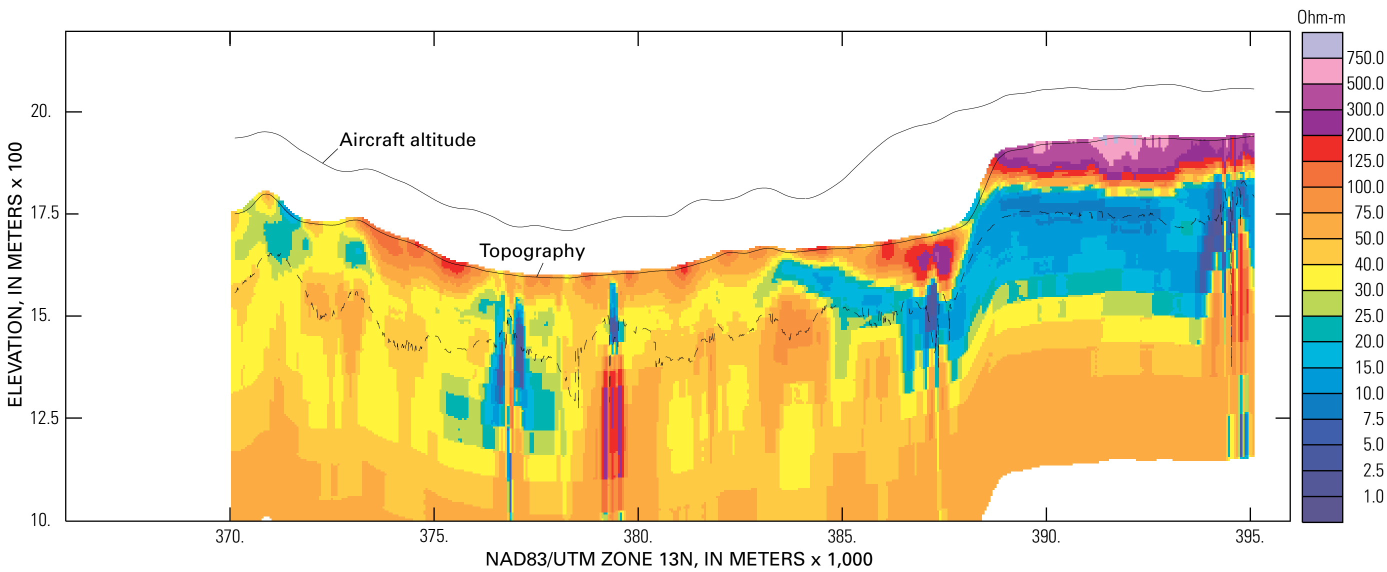

Figure F10. Resistivity under flight line 630 in the Cochiti Pueblo time-domain electromagnetic survey area, drawn on the basis of least-squares inversion. Line floating above cross section represents aircraft altitude; faint dashed line represents maximum depth estimated from resistivity-depth image (fig. F9). Vertical exaggeration is 10.

Figure F11 (following 3 pages). East-west resistivity profiles in the Cochiti Pueblo time-domain electromagnetic survey area (cross sections F14*A*–*G*), drawn on the basis of least-squares inversions. Faint dashed line in each section represents maximum depth estimated from resistivity-depth image; numbers below magnetotelluric (MT) or audiomagnetotellurid (AMT) stations refer to modeled resistivities. Vertical exaggeration is 10. *A*, Flight line 605 showing Dome Road well and MT station 17. *B,* Flight line 609 showing AMT stations 1, 6, and 5 and Cochiti Lake 2 and 1200-Foot wells. *C*, Flight line 614 showing AMT station 2. *D*, Flight line 630 showing AMT stations 3 and 4, magnetic anomalies C3 and C4, and Santa Cruz Springs well. *E*, Flight line 638 showing Mancos Shale in footwall block of La Bajada fault zone. *F*, Flight line 643 showing Cerrillos uplift in footwall block of La Bajada fault zone. *G*, Flight line 626 showing magnetic anomaly C5.

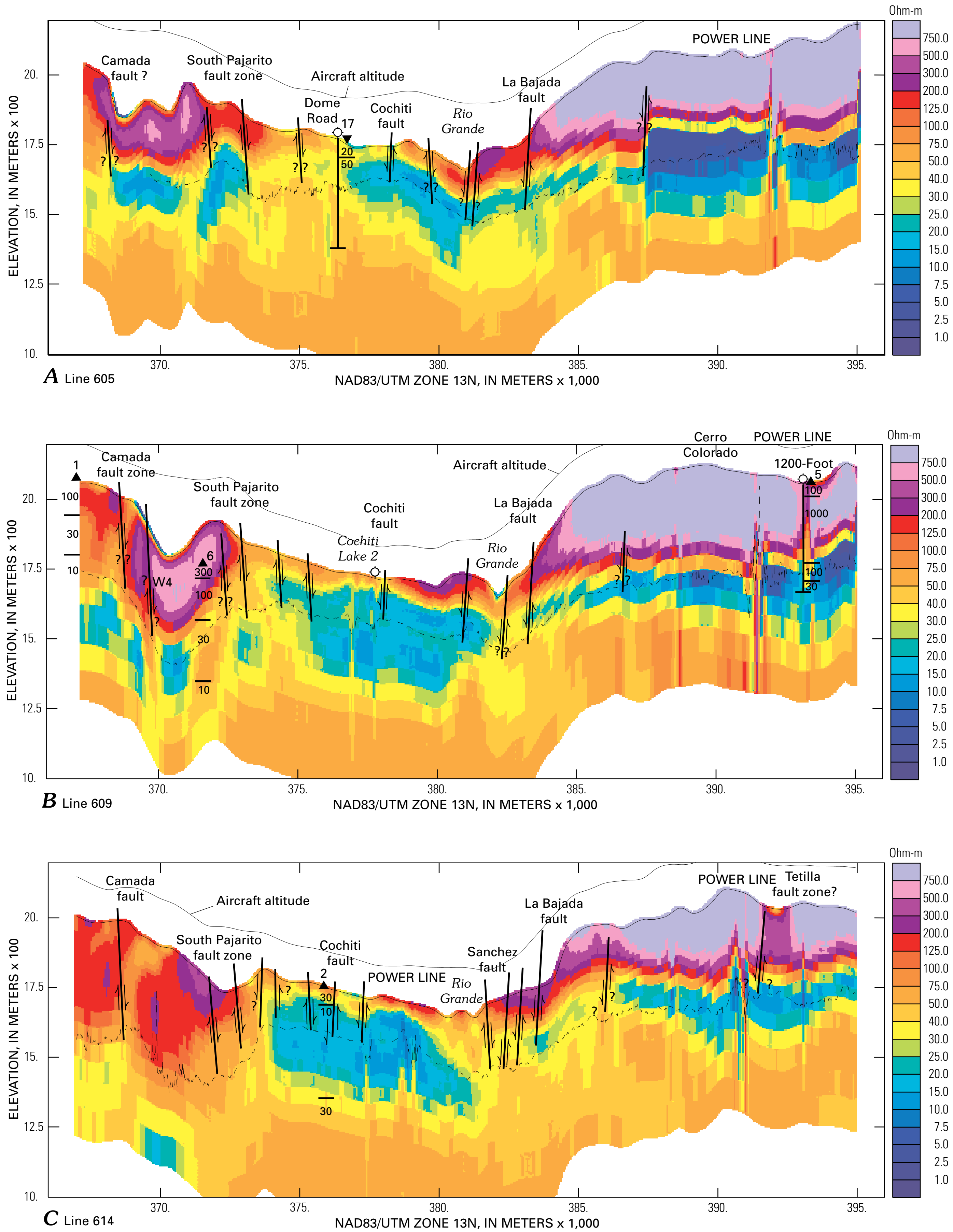

Ohm-m
750.0
500.0
300.0
200.0
125.0
100.0
75.0
50.0
40.0
30.0
25.0
20.0
15.0
10.0
7.5
5.0
2.5
1.0
ELEVATION, IN METERS x 100
20.
17.5
15.
12.5
10.
370.
375.
380.
385.
390.
395.
NAD83/UTM ZONE 13N, IN METERS x 1,000
Camada fault ?
South Pajarito fault zone
Aircraft altitude
Dome Road
17
20
50
Cochiti fault
Rio Grande
La Bajada fault
POWER LINE
A Line 605
1
100
30
10
Camada fault zone
South Pajarito fault zone
W4
6
300
100
30
10
Cochiti fault
Cochiti Lake 2
Aircraft altitude
La Bajada fault
Rio Grande
Cerro Colorado
POWER LINE
1200-Foot
5
100
1000
100
30
B Line 609
Camada fault
Aircraft altitude
South Pajarito fault zone
Cochiti fault
2
30
10
30
POWER LINE
Rio Grande
Sanchez fault
La Bajada fault
POWER LINE
Tetilla fault zone?
C Line 614

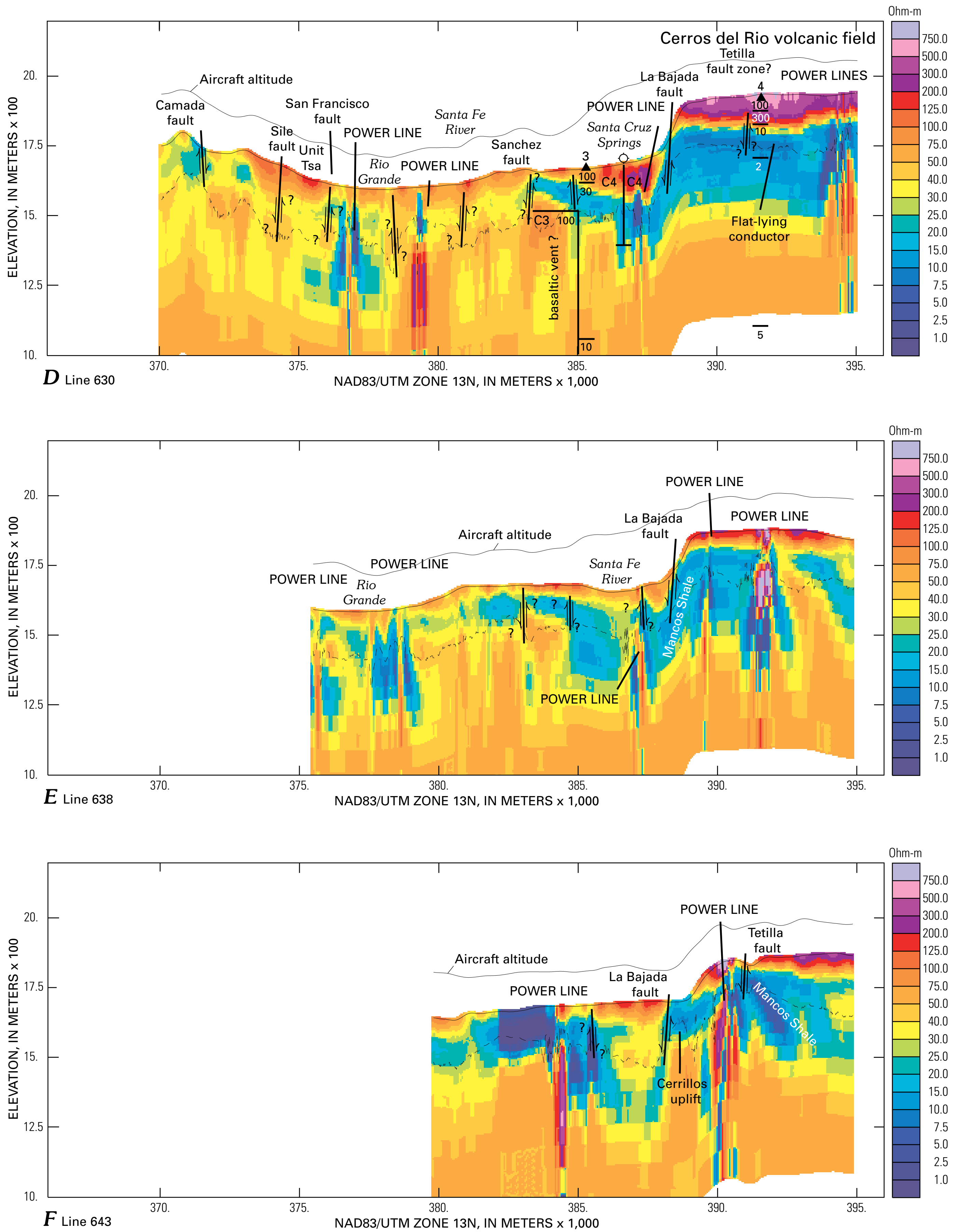
Ohm-m
750.0
500.0
300.0
200.0
125.0
100.0
75.0
50.0
40.0
30.0
25.0
20.0
15.0
10.0
7.5
5.0
2.5
1.0
Cerros del Rio volcanic field
Tetilla
fault zone?
POWER LINES
Aircraft altitude
La Bajada
fault
Camada
fault
San Francisco
fault
POWER LINE
Santa Fe
River
Santa Cruz
Springs
Sile
fault
Unit
Tsa
Rio
Grande
POWER LINE
Sanchez
fault
C3
C4
C4
basaltic vent ?
Flat-lying
conductor
ELEVATION, IN METERS x 100
NAD83/UTM ZONE 13N, IN METERS x 1,000
D Line 630
POWER LINE
La Bajada
fault
POWER LINE
Aircraft altitude
POWER LINE
Santa Fe
River
POWER LINE
Rio
Grande
Mancos Shale
POWER LINE
E Line 638
POWER LINE
Tetilla
fault
Aircraft altitude
La Bajada
fault
POWER LINE
Mancos Shale
Cerrillos
uplift
F Line 643

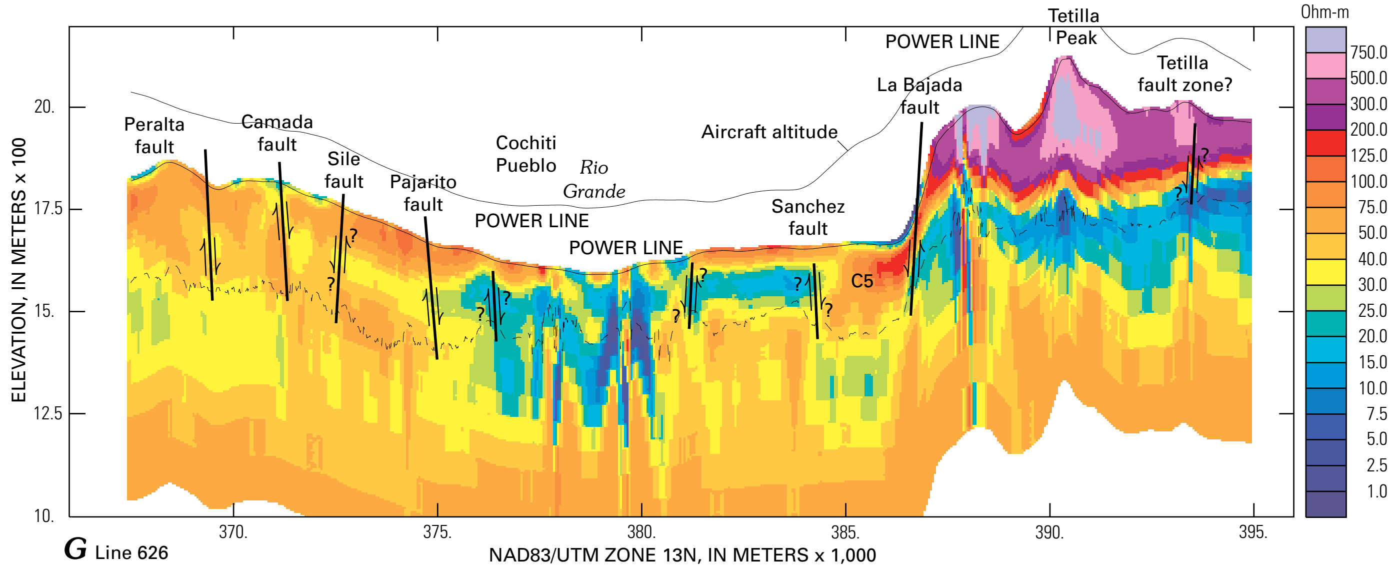

least 100 m thick lay above the resistivity-depth-image limit) and also in the upper 50 m (where the least-squares inversion close to the surface generally yields resistivities higher than the shallowest AMT resistivities). AMT data suggest that some inversion resistivities below the resistivity-depth-image limit are still valid (especially when a thick section of resistive material lies above the resistivity-depth-image depth limit). Rather than plotting as a blank area the resistivity values below the resistivity-depth-image depth limit on the resistivity cross sections, we included all values of the inversion. So doing allowed us to view those cases where a conductor exists beneath a thick section of resistive materials but below the resistivity-depth image-depth limit (for example, below the magnetic anomaly labeled C5 in fig. F11*G*; refer to fig. D7). We are of the opinion that in these cases the TDEM response is sensitive to the conductor at depth below the thick resistor, even though that conductor is below the resistivity-depth-image depth limit. However, the basement resistivity was fixed at 50 ohm-m, so interpretations should not use the last resistivity gradient between the basement resistivity of 50 ohm-m and the shallower resistivity feature in question.

By using the line-by-line least-squares inversions found by the above procedures, plan maps of resistivity were generated for the survey area by combining the least-squares inversion cross sections into a three-dimensional grid of resistivity. Resistivities below the maximum resistivity-depth-image depth limit were set to plot a blank area. Areas that were either outside the survey region or were at elevations above the ground surface were also plotted as blank areas. Horizontal depth-slice maps of resistivity (fig. F12*A–F*) at 50 m elevation intervals were generated from the least-squares inversion results along each of the flight lines. Elevations mapped were 1,750, 1,700, 1,550, 1,500, 1,450 and 1,400 m above sea level (elevations 1,550, 1,500, 1,450, and 1,400 m are marked by thin, horizontal lines on fig. F9). Figure F7*A–F* shows resistivity maps (also generated from the same least-squares inversion results) at constant depths below the surface (20, 50, 70, 100, 150 and 200 m) draped on topography. We did not use the resistivity-depth image results to produce the depth-slice maps because the resistivities derived from the resistivity-depth image algorithm generally did not extend to the surface and did not correlate very well with the AMT soundings in the upper 50 to 100 m (for example, fig. F11*D*). Vertical cross sections from the least-squares inversions were generated along each of the 50 east-west flight lines and for 8 north-south flight lines. Selected profiles are depicted in figures F11 and F13.

Geologic Interpretation of Airborne Electromagnetic Models

The TDEM survey objectives, defined in the preceding Time-Domain Electromagnetic Survey section, were based on the assumption that the axial-river gravel deposits, which are the

Figure F12 (followin 6 pages). Elevation slices in the Cochiti Pueblo time-domain electromagnetic survey area (*A–F*), drawn on the basis of least-squares inversions. Solid numbered triangles are high-frequency magnetotelluric (AMT) sounding stations. Labels C, M, and F are inferred sedimentary grain size: coarse, medium, and fine, respectively. V marks inferred volcanic rock. Inferred grain size labels appear only on elevation slices below the water table (*C–F*); approximate boundaries are shown by lighter dashed lines. *A,* 1,750-m elevation slice. *B*, 1,700-m elevation slice. *C*, 1,550-m elevation slice. *D*, 1,500-m elevation slice. *E*, 1,450-m elevation slice. *F*, 1,400-m elevation slice.

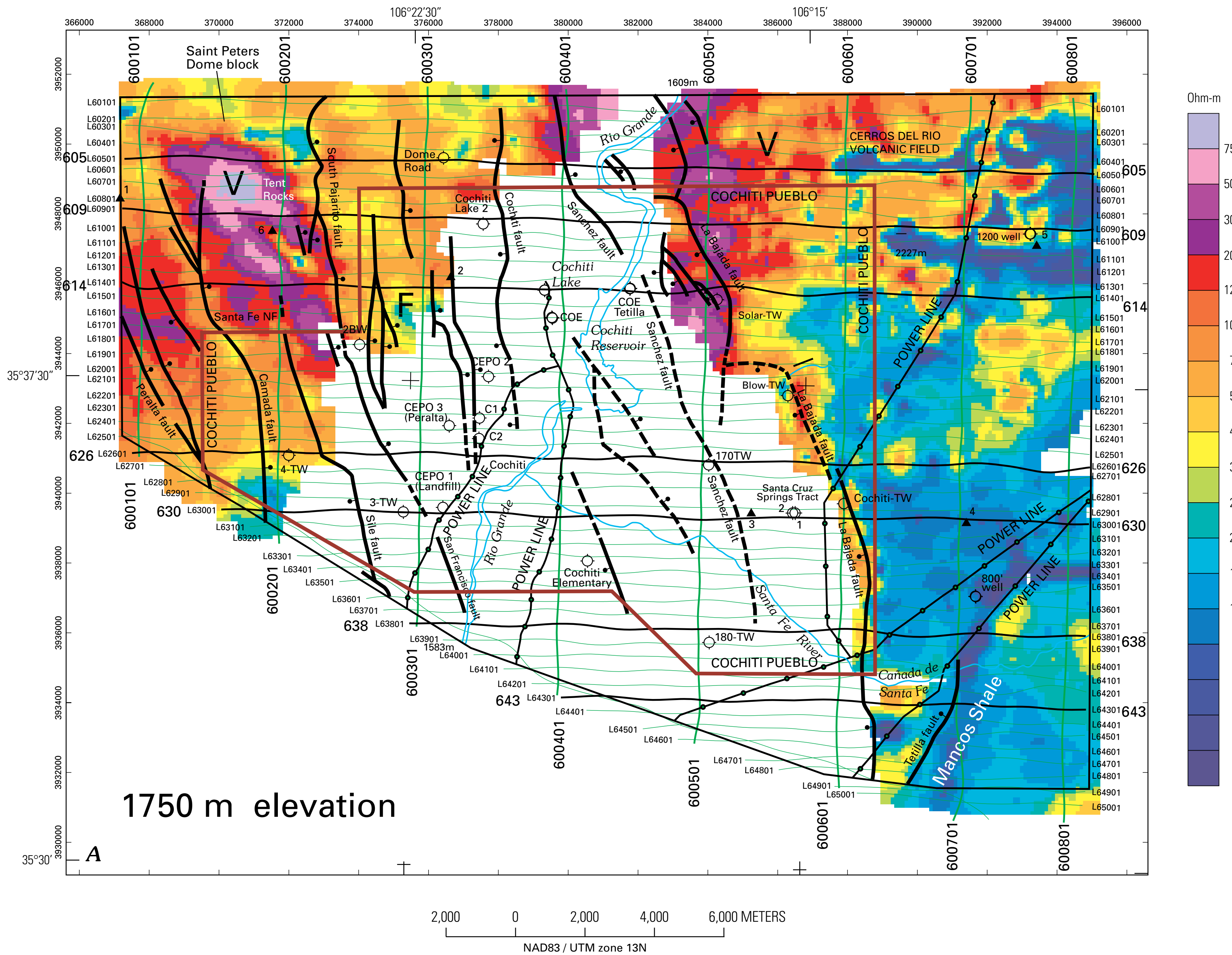
1750 m elevation
A
Ohm-m
750.0
500.0
300.0
200.0
125.0
100.0
75.0
50.0
40.0
30.0
25.0
20.0
15.0
10.0
7.5
5.0
2.5
1.0
2,000 0 2,000 4,000 6,000 METERS
NAD83 / UTM zone 13N
106°22'30"
106°15'
35°37'30"
35°30'
Saint Peters Dome block
Tent Rocks
CERROS DEL RIO VOLCANIC FIELD
COCHITI PUEBLO
Rio Grande
Dome Road
Cochiti Lake 2
Cochiti Lake
COE Tetilla
COE
Cochiti Reservoir
Santa Fe NF
South Pajarito fault
Cochiti fault
Sanchez fault
La Bajada fault
Peralta fault
Canada fault
Sile fault
San Francisco fault
Tetilla fault
Mancos Shale
POWER LINE
Solar-TW
Blow-TW
170TW
180-TW
Cochiti-TW
Santa Cruz Springs Tract
1200 well
800' well
2227m
1609m
1583m
CEPO 2
CEPO 3 (Peralta)
CEPO 1 (Landfill)
C1
C2
Cochiti
Cochiti Elementary
2BW
3-TW
4-TW
Santa Fe River
Cañada de Santa Fe
605
609
614
626
630
638
643
600101
600201
600301
600401
600501
600601
600701
600801

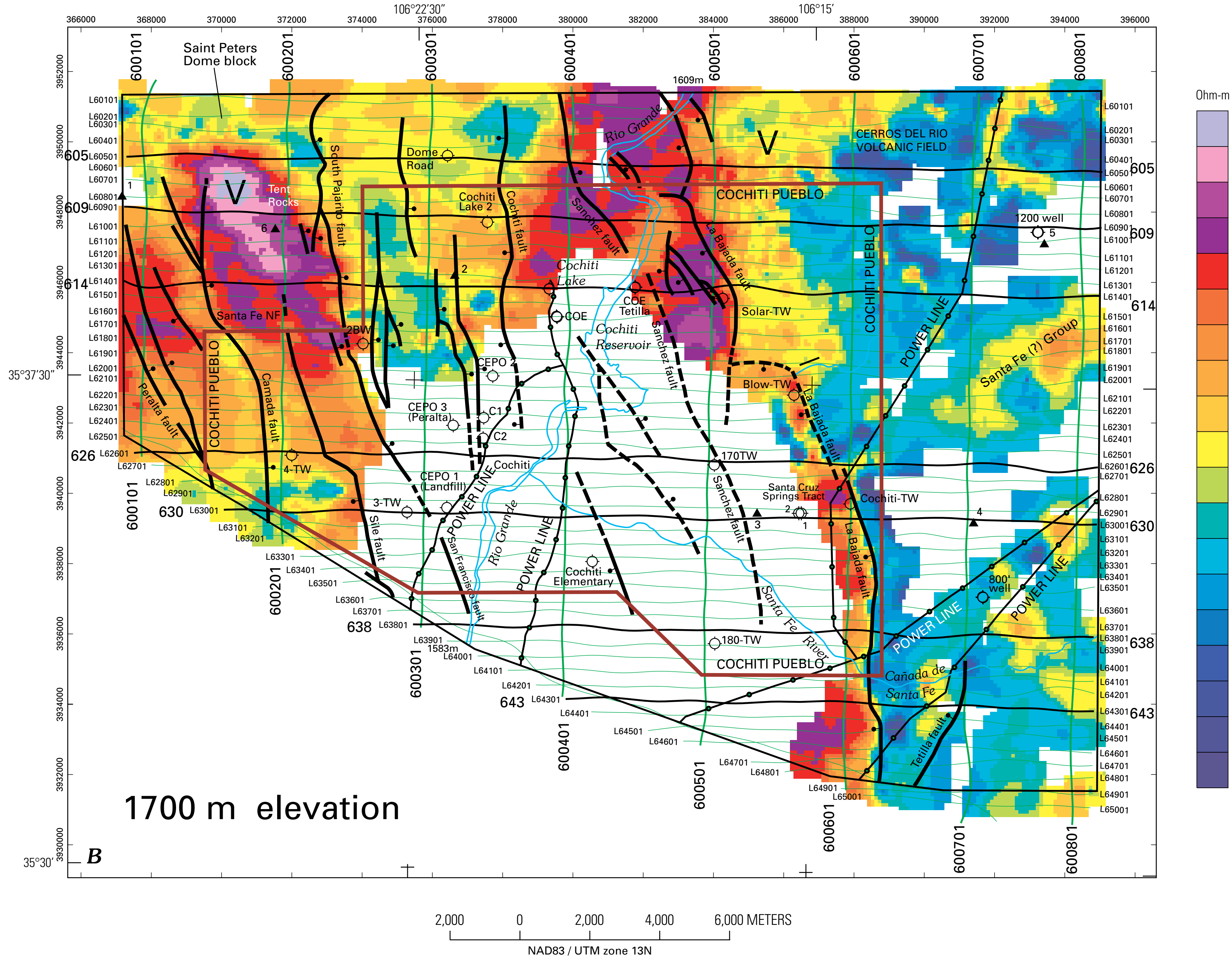

106°22'30"
106°15'
35°37'30"
35°30'
Saint Peters Dome block
Tent Rocks
Dome Road
Cochiti Lake 2
COCHITI PUEBLO
CERROS DEL RIO VOLCANIC FIELD
1200 well
1609m
Rio Grande
Sanchez fault
La Bajada fault
Cochiti fault
South Pajarito fault
Cochiti Lake
COE
COE Tetilla
Solar-TW
Cochiti Reservoir
Santa Fe NF
2BW
CEPO 2
CEPO 3 (Peralta)
C1
C2
CEPO 1 (Landfill)
Cochiti
Blow-TW
170TW
Santa Cruz Springs Tract
Cochiti-TW
Peralta fault
Canada fault
4-TW
3-TW
Sile fault
San Francisco fault
POWER LINE
Cochiti Elementary
Santa Fe River
180-TW
1583m
800' well
Cañada de Santa Fe
Tetilla fault
Santa Fe (?) Group
1700 m elevation
B
Ohm-m
750.0
500.0
300.0
200.0
125.0
100.0
75.0
50.0
40.0
30.0
25.0
20.0
15.0
10.0
7.5
5.0
2.5
1.0
2,000
0
2,000
4,000
6,000 METERS
NAD83 / UTM zone 13N

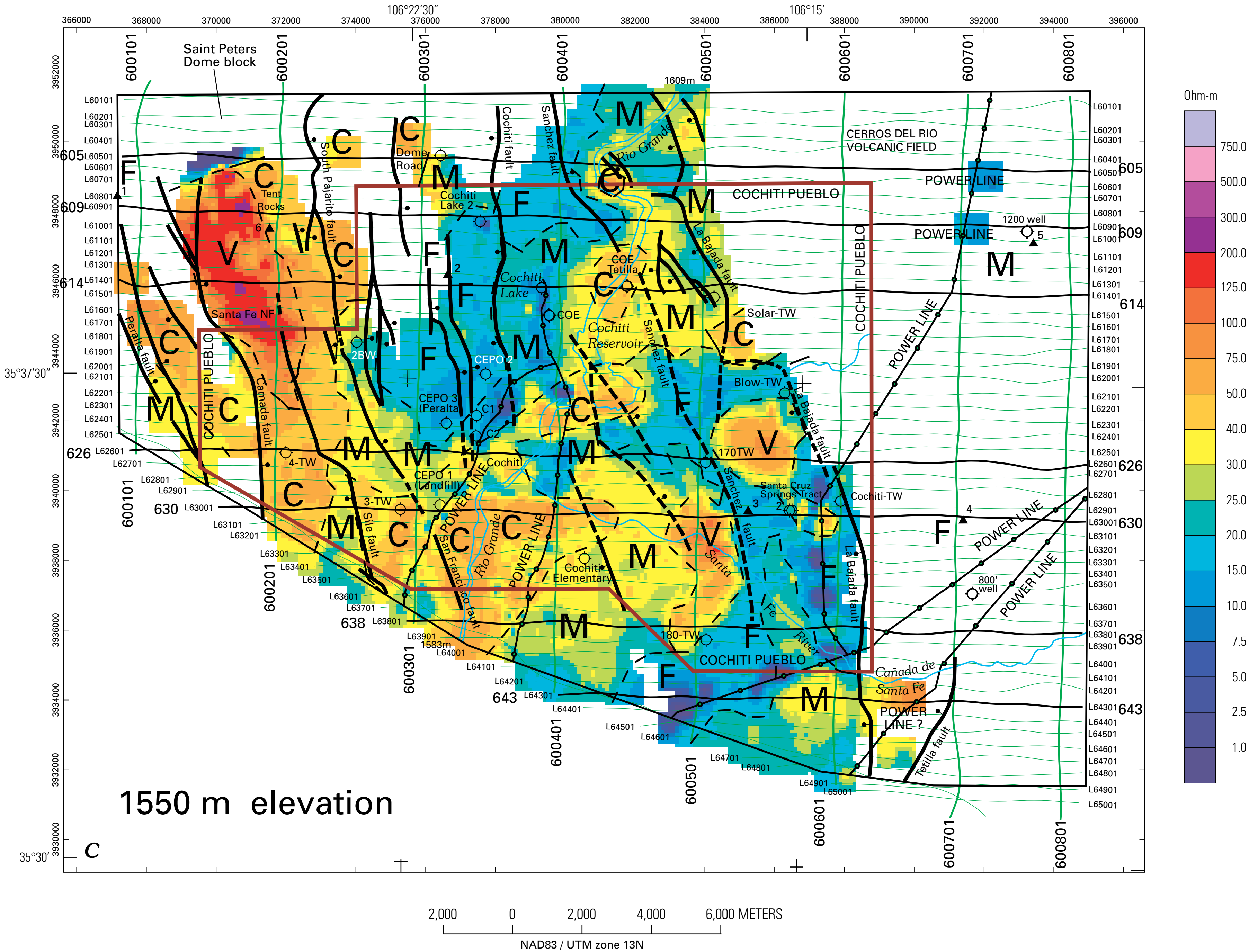
1550 m elevation
c
Ohm-m
750.0
500.0
300.0
200.0
125.0
100.0
75.0
50.0
40.0
30.0
25.0
20.0
15.0
10.0
7.5
5.0
2.5
1.0
106°22'30"
106°15'
35°37'30"
35°30'
Saint Peters Dome block
CERROS DEL RIO VOLCANIC FIELD
COCHITI PUEBLO
POWER LINE
1200 well
800' well
Tent Rocks
Santa Fe NF
Dome Road
Cochiti Lake 2
Cochiti Lake
COE
COE Tetilla
Cochiti Reservoir
Solar-TW
Blow-TW
170TW
Santa Cruz Springs Tract
Cochiti-TW
CEPO 2
CEPO 3 (Peralta)
CEPO 1 (Landfill)
Cochiti
Cochiti Elementary
2BW
4-TW
3-TW
180-TW
1609m
1583m
Rio Grande
Santa Fe River
Cañada de Santa Fe
South Pajarito fault
Cochiti fault
Sanchez fault
La Bajada fault
Sanchez fault
Peralta fault
Camada fault
Sile fault
San Francisco fault
Tetilla fault
POWER LINE ?
605
609
614
626
630
638
643
2,000 0 2,000 4,000 6,000 METERS
NAD83 / UTM zone 13N

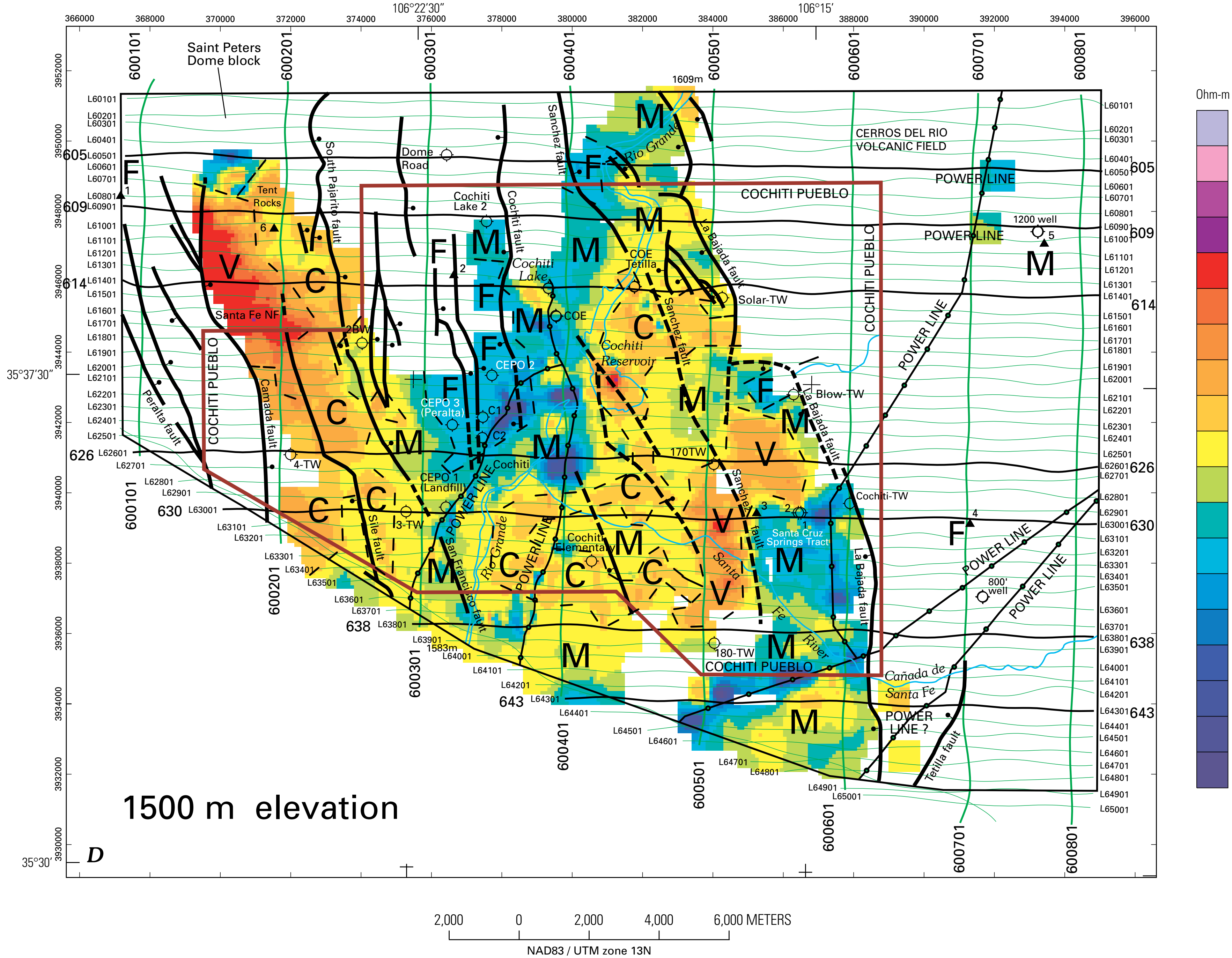
106°22'30"
106°15'
35°37'30"
35°30'
Saint Peters Dome block
Tent Rocks
Santa Fe NF
COCHITI PUEBLO
CERROS DEL RIO VOLCANIC FIELD
POWER LINE
1200 well
Dome Road
Cochiti Lake 2
Cochiti Lake
COE Tetilla
COE
Solar-TW
Cochiti Reservoir
CEPO 2
CEPO 3 (Peralta)
CEPO 1 (Landfill)
Cochiti
Cochiti Elementary
Blow-TW
170TW
Cochiti-TW
Santa Cruz Springs Tract
4-TW
3-TW
2BW
180-TW
800' well
1609m
1583m
Peralta fault
Camada fault
South Pajarito fault
Cochiti fault
Sanchez fault
La Bajada fault
Sile fault
San Francisco fault
Tetilla fault
Rio Grande
Santa Fe River
Cañada de Santa Fe
POWER LINE ?
1500 m elevation
D
Ohm-m
750.0
500.0
300.0
200.0
125.0
100.0
75.0
50.0
40.0
30.0
25.0
20.0
15.0
10.0
7.5
5.0
2.5
1.0
2,000
0
2,000
4,000
6,000 METERS
NAD83 / UTM zone 13N

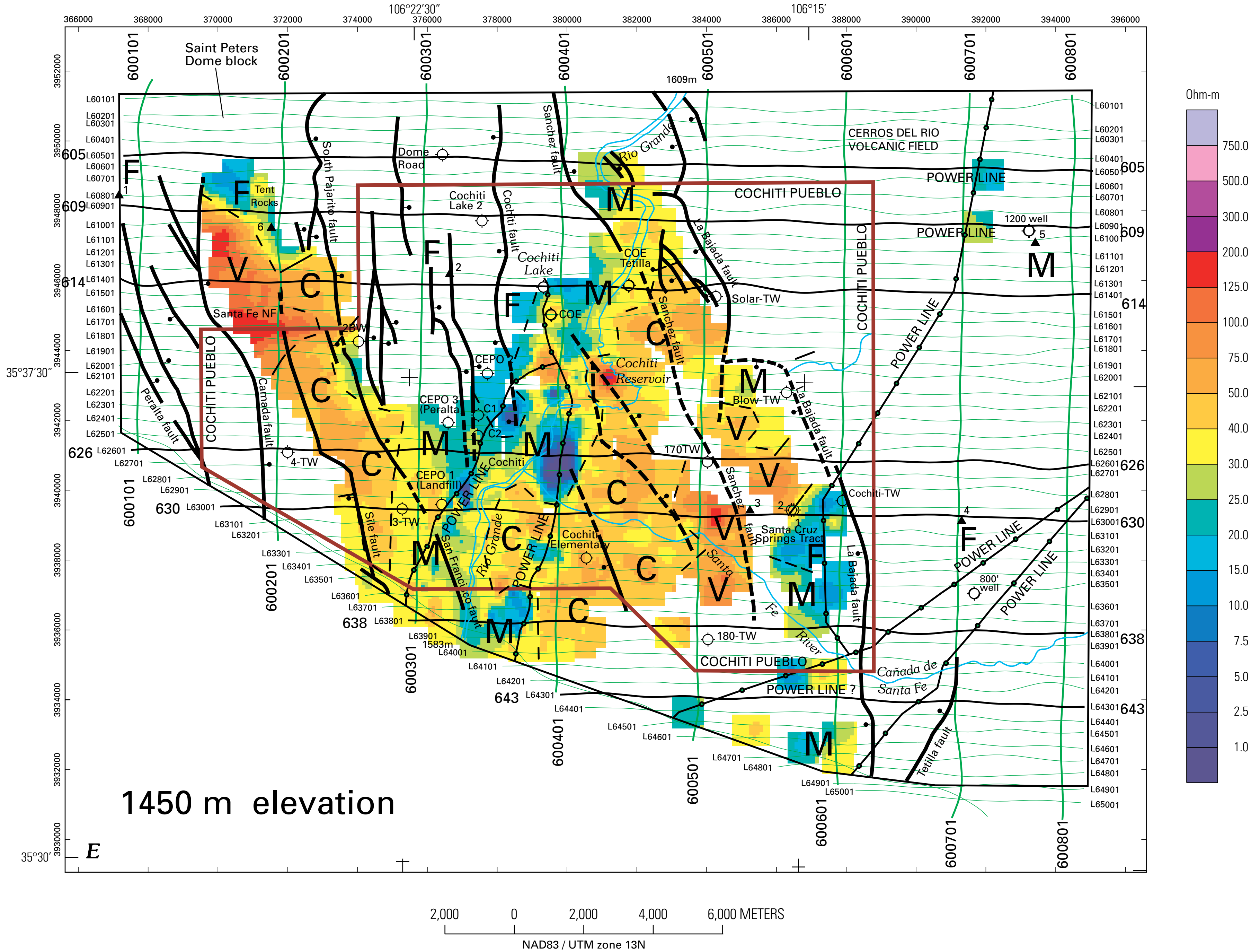
1450 m elevation
E
Ohm-m
750.0
500.0
300.0
200.0
125.0
100.0
75.0
50.0
40.0
30.0
25.0
20.0
15.0
10.0
7.5
5.0
2.5
1.0
106°22'30"
106°15'
35°37'30"
35°30'
Saint Peters Dome block
CERROS DEL RIO VOLCANIC FIELD
COCHITI PUEBLO
POWER LINE
POWER LINE ?
Tent Rocks
Santa Fe NF
Dome Road
Cochiti Lake 2
Cochiti Lake
COE Tetilla
COE
Solar-TW
Cochiti Reservoir
Blow-TW
170TW
Cochiti-TW
1200 well
800' well
CEPO
CEPO 3 (Peralta)
CEPO 1 (Landfill)
Cochiti
Cochiti Elementary
Santa Cruz Springs Tract
2BW
4-TW
3-TW
180-TW
1609m
1583m
Rio Grande
Santa Fe River
Cañada de Santa Fe
South Pajarito fault
Cochiti fault
Sanchez fault
La Bajada fault
Peralta fault
Camada fault
Sile fault
San Francisco fault
Tetilla fault
2,000 0 2,000 4,000 6,000 METERS
NAD83 / UTM zone 13N

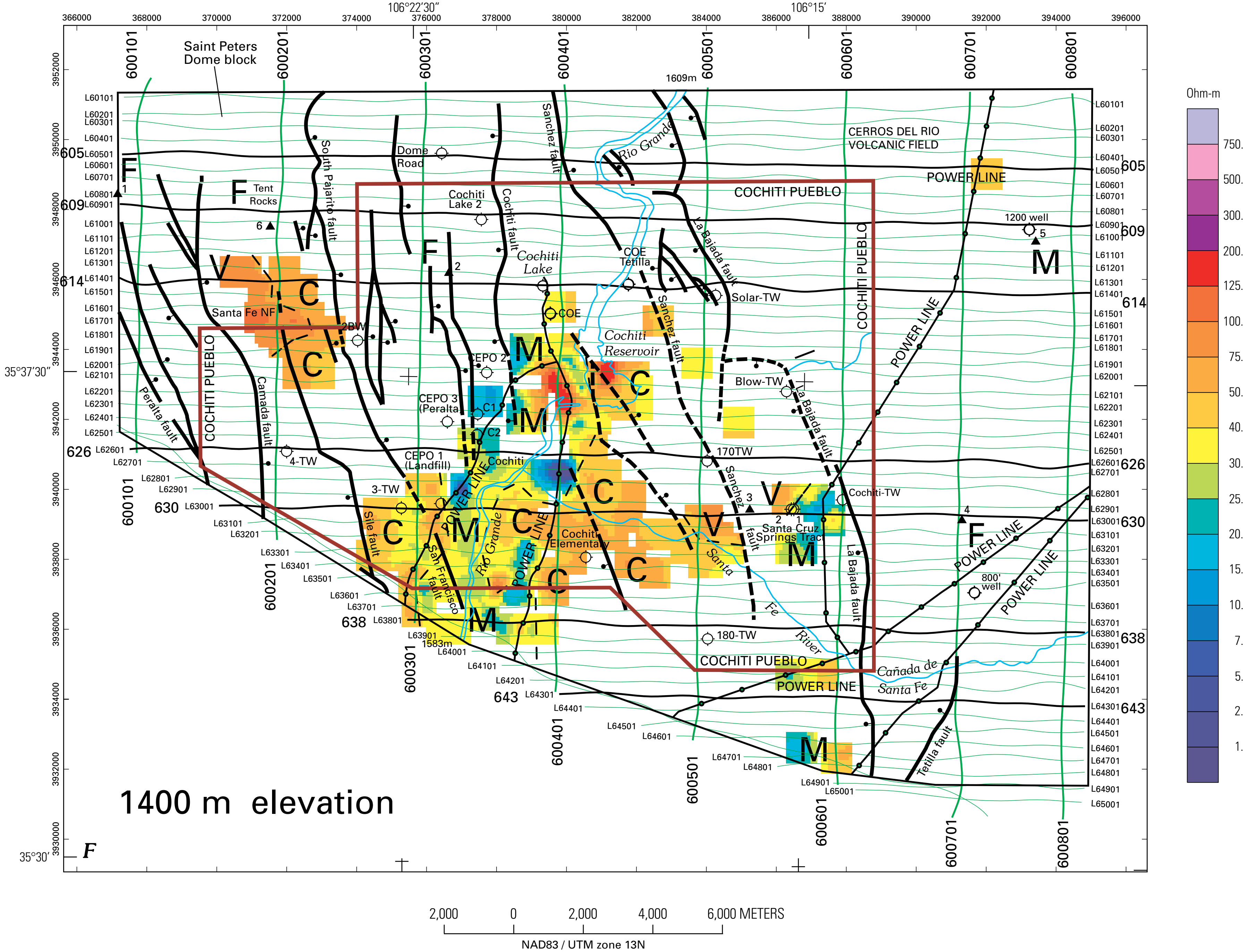
106°22'30"
106°15'
366000
368000
370000
372000
374000
376000
378000
380000
382000
384000
386000
388000
390000
392000
394000
396000
3952000
3950000
3948000
3946000
3944000
3942000
3940000
3938000
3936000
3934000
3932000
3930000
35°37'30"
35°30'
600101
600201
600301
600401
600501
600601
600701
600801
605
609
614
626
630
638
643
Saint Peters
Dome block
1609m
CERROS DEL RIO
VOLCANIC FIELD
POWER LINE
COCHITI PUEBLO
Dome
Road
Cochiti
Lake 2
Tent
Rocks
South Pajarito fault
Cochiti fault
Sanchez fault
Rio Grande
La Bajada fault
Cochiti
Lake
COE
Tetilla
Solar-TW
1200 well
Santa Fe NF
2BW
COE
Cochiti
Reservoir
CEPO 2
C1
C2
CEPO 3
(Peralta)
Blow-TW
Peralta fault
Camada fault
4-TW
CEPO 1
(Landfill)
Cochiti
170TW
Cochiti-TW
3-TW
Sile fault
San Francisco
fault
Cochiti
Elementary
Santa Cruz
Springs Tract
800'
well
1583m
180-TW
Santa Fe River
Cañada de
Santa Fe
Tetilla fault
1400 m elevation
F
V
C
M
Ohm-m
750.0
500.0
300.0
200.0
125.0
100.0
75.0
50.0
40.0
30.0
25.0
20.0
15.0
10.0
7.5
5.0
2.5
1.0
2,000
0
2,000
4,000
6,000 METERS
NAD83 / UTM zone 13N

main aquifers in the middle Rio Grande Basin (Bartolino, 1999), will have a higher electrical resistivity than surrounding finer grained materials (Hearst, Nelson, and Paillet, 2000). However, the resistivities obtained from TDEM are only indirectly related to the water content and the sediment grain size at depth, and they must be correlated with other geologic information.

The correlation of TDEM inversion resistivities with grain size within the Santa Fe Group sediments was possible with the help of induction and lithologic logs from wells in the survey area. To make the correlation reliable, the well had to meet three criteria: be within 200 m of the nearest flight line, have both induction and lithologic logs in the same depth range as the TDEM survey, and be at least 200 m away from cultural noise (using a cutoff value of 10,000 microvolts) owing to power lines, pipelines, or other man-made electrical power sources. Only four logged wells lay within areas covered by airborne surveys (Deszcz-Pan and others, 2000) met criteria for reliability. Three wells are in Rio Rancho (survey area A+B, fig. F1); one well (CEPO 2, fig. F2*A*; induction log, fig. F8*B*) was in Cochiti Pueblo (survey area D, fig. F1). Deszcz-Pan and others (2000) showed that one-dimensional inversion algorithms, developed and owned by BHP World Minerals, provided resistivity cross sections that closely correlate with the Rio Rancho well logs. The resistivity inversion also closely correlates with the one Cochiti Pueblo well log (CEPO 2, fig. F2*A*) below the static water level (SWL, fig. F8*B*). Above the static water level (upper 37 m (120 ft)), the inversion resistivity underestimated the induction log resistivity. The underestimation probably reflects the influence of an adjacent shallow conductor (20 ohm-m) just south of CEPO 2 (fig. F7*A*) that dips underneath CEPO 2 at 50 m (165 ft) depth (fig. F7*B*). Also, at 84–102 m (275–335 ft) depth, the inversion did not resolve the interval, 9–12 m (30–40 ft) thick, of moderately resistive coarse-grained sediments (60 ohm-m) (fig. F8*B*). This failure indicates that TDEM inversion for this survey was able to resolve only those resistive units whose thickness is greater than about 15 percent of their burial depth. Except for this resolution limitation and the underestimated resistivity in the upper 37 m (120 ft), the inversion correlates well with lithologic grain size below the water table.

Resistivities were correlated with grain size only in the saturated zone (Deszcz-Pan and others, 2000), owing to the lack of information about partial saturation in the vadose zone. Deszcz-Pan and others (2000) correlated resistivity and grain size in the saturated zone as follows: coarse grain size (40–70 ohm-m), medium grain size (20–40 ohm-m), and fine grain size (10–20 ohm-m). We also observed changes in TDEM response at several faults mapped at the surface (figs. F7, F12) and at faults inferred from a high-resolution airborne magnetic survey (Grauch, 1999; chapter D, this volume), delineating pronounced changes in lithology in Santa Fe Group sediments owing to fault juxtapositions. Variations in the pattern of resistivity can thus be linked to hydrostratigraphic changes across faults, including growth-fault-related facies variations in sediments of the Santa Fe Group and contemporaneous volcanic deposits.

The resistivity models obtained by the airborne TDEM survey correlate with the three principal geologic terranes in the La Bajada constriction area depicted in figure A4. Basaltic rocks of the Cerros del Rio volcanic field, in the footwall of the La Bajada fault zone (fig. F7), are characterized by very high resistivities (>500–750 ohm-m). Higher resistivity areas generally correspond with vent areas of individual volcanoes. The tapering edges of unsaturated thin basalts generally have resistivities of 30–100 ohm-m. The southern boundary of the resistive basalts dips north and is bounded by conductive sedimentary rocks. However, the increase in thickness of the >100 ohm-m resistive section (fig. F14*A*) correlates with higher elevation cones and vents within the Cerros del Rio volcanic field. Comparison of the thickness diagram with a map of the calculated base of the resistive section (fig. F14*B*) clearly shows that most of the thickening pattern is due to increasing constructional topography of the Cerros del Rio volcanoes. As determined by results from AMT station 5 and the 1200-Foot well (fig. F4*B*), both the volcanic lavas and the Santa Fe Group sediments thicken to the north (see also geologic cross sections, pl. 6). The east-dipping Mancos Shale is distinctive in the depth slices at 70 and 100 ohm-m (fig. F7*C*, *D*) just east of the Tetilla fault zone, where resistivity for this very conductive marine shale is below 7.5 ohm-m. The east-dipping Mancos Shale can also be seen in cross section in the 643 TDEM resistivity profile (fig. F11*F*) east of the Tetilla fault zone. On the TDEM 1,750-m elevation-slice map (fig. F12*A*), south of the northeast-trending power line and south of flight line 638, the Tetilla fault zone appears to form the western boundary of the east-dipping conductive Mancos Shale. The resistivity character of the Cerros del Rio area north of the two northeast-trending power lines, near AMT station 4, appears to differ from that south of the power lines. North of the power lines, the east-dipping conductive material on the 630 TDEM resistivity profile (fig. F11*D*) is gone, and minor breaks disrupt what otherwise appear to be fairly flat-lying conductive layers. The 1,700-m-elevation TDEM slice map (fig. F12*B*) depicts moderately resistive material surrounded by moderately conductive material, which suggests a structural block between AMT stations 4 and 5 at a bearing of about N. 60° E. The structure of this block can also be seen north of AMT station 4 in the north-south 600701 TDEM resistivity profile (fig. F13*G*) and south of AMT station 5 in the north-south 600801 TDEM resistivity profile (fig. F13*H*). The moderately resistive character of this section is similar to that of sediments in the Santa Fe Group.

The western terrane, Saint Peters Dome block (figs. F12, F7), also displays high resistivity values in the footwall block of the Pajarito fault zone, and those higher resistivities continue south into the Santo Domingo Basin between the Pajarito and Sile faults. In the west, an exposed rhyolite dome and related pyroclastic deposits near Tent Rocks (V, figs. F12, F7) have high resistivities. The dome and pyroclastic deposits have peak resistivities greater than 500–750 ohm-m in the depth range of 100–150 m below the surface, so their highest values are more limited here than in the basaltic rocks of the Cerros

Figure F13 (below and following 2 pages). North-south profiles in the Cochiti Pueblo time-domain electromagnetic survey area (cross sections *A*–*H*), drawn on the basis of least-squares inversions. Dashed line in each section is maximum depth estimated from resistivity-depth image; numbers below wells or stations represent modeled resistivities. Vertical exaggeration is 10. *A,* Flight line 600101 showing audiomagnetotelluric (AMT) station 1. *B*, Flight line 600201 showing AMT station 6. *C,* Flight line 600301 showing Dome Road well. *D*, Flight line 600401 showing Sanchez fault. *E*, Flight line 600501 showing La Bajada fault zone. *F*, Flight line 600601 showing La Bajada fault zone. *G*, Flight line 600701 showing AMT station 4. *H*, Flight line 600801 showing AMT station 5 and 1200-Foot well.

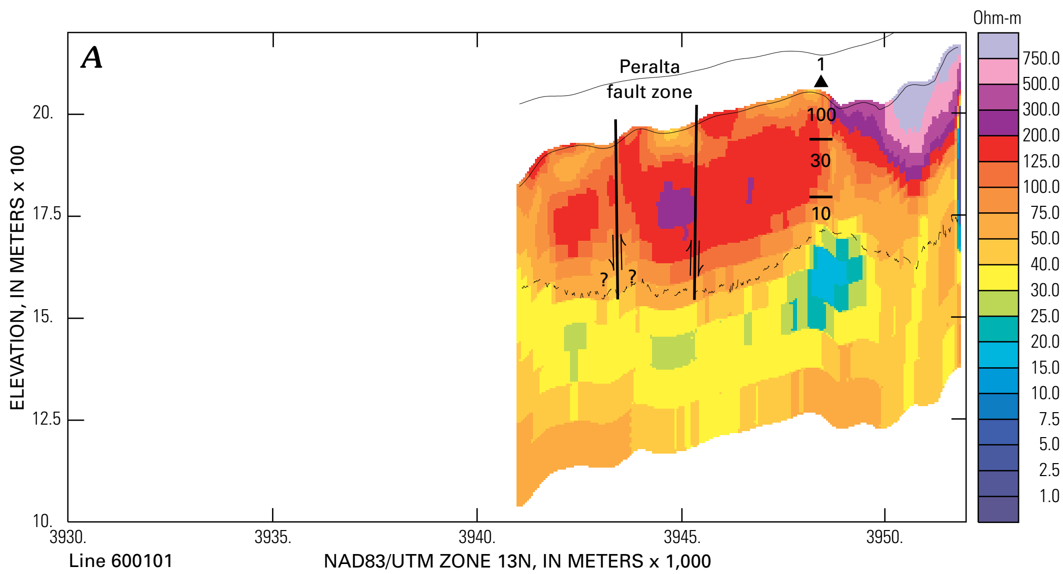

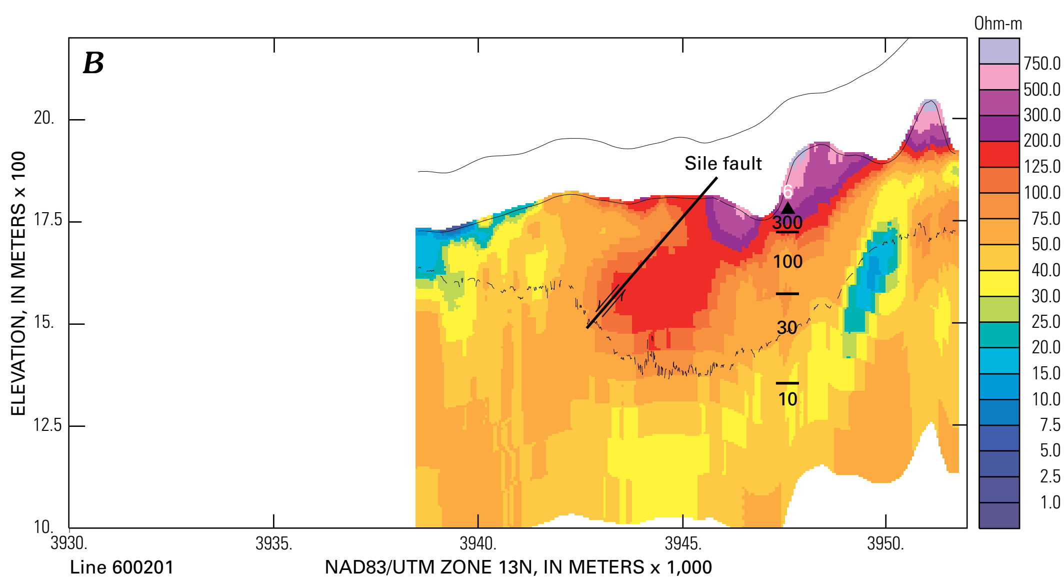

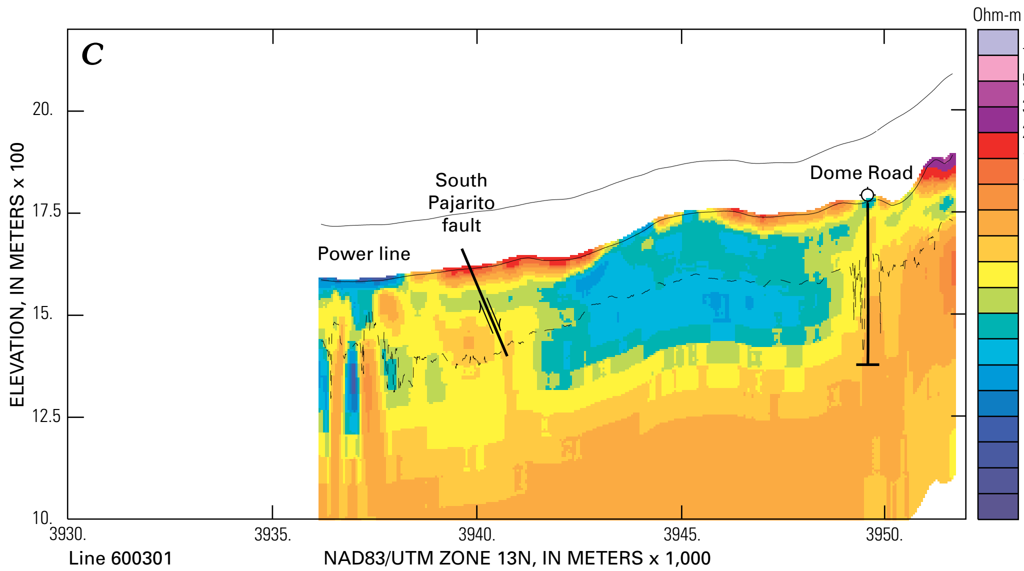
C
Ohm-m
750.0
500.0
300.0
200.0
125.0
100.0
75.0
50.0
40.0
30.0
25.0
20.0
15.0
10.0
7.5
5.0
2.5
1.0
South
Pajarito
fault
Power line
Dome Road
ELEVATION, IN METERS x 100
20.
17.5
15.
12.5
10.
3930.
3935.
3940.
3945.
3950.
Line 600301
NAD83/UTM ZONE 13N, IN METERS x 1,000

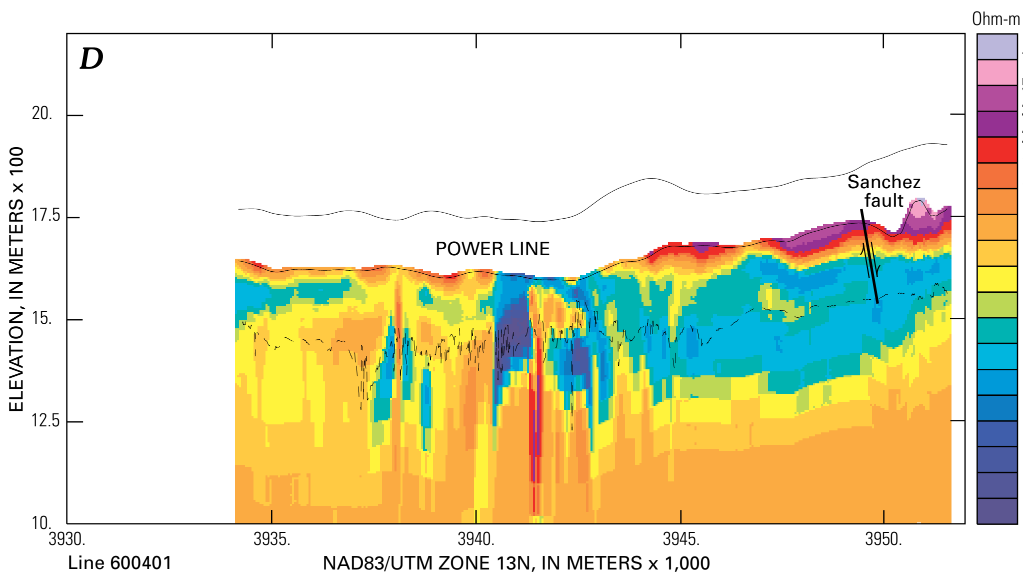
D
Ohm-m
750.0
500.0
300.0
200.0
125.0
100.0
75.0
50.0
40.0
30.0
25.0
20.0
15.0
10.0
7.5
5.0
2.5
1.0
Sanchez
fault
POWER LINE
ELEVATION, IN METERS x 100
20.
17.5
15.
12.5
10.
3930.
3935.
3940.
3945.
3950.
Line 600401
NAD83/UTM ZONE 13N, IN METERS x 1,000

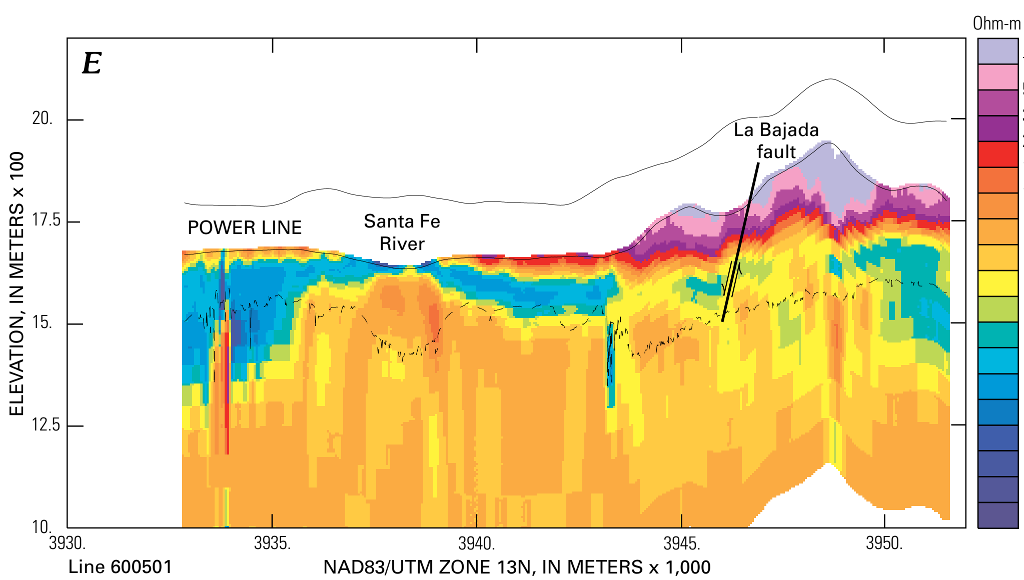
E
Ohm-m
750.0
500.0
300.0
200.0
125.0
100.0
75.0
50.0
40.0
30.0
25.0
20.0
15.0
10.0
7.5
5.0
2.5
1.0
La Bajada
fault
POWER LINE
Santa Fe
River
ELEVATION, IN METERS x 100
20.
17.5
15.
12.5
10.
3930.
3935.
3940.
3945.
3950.
Line 600501
NAD83/UTM ZONE 13N, IN METERS x 1,000

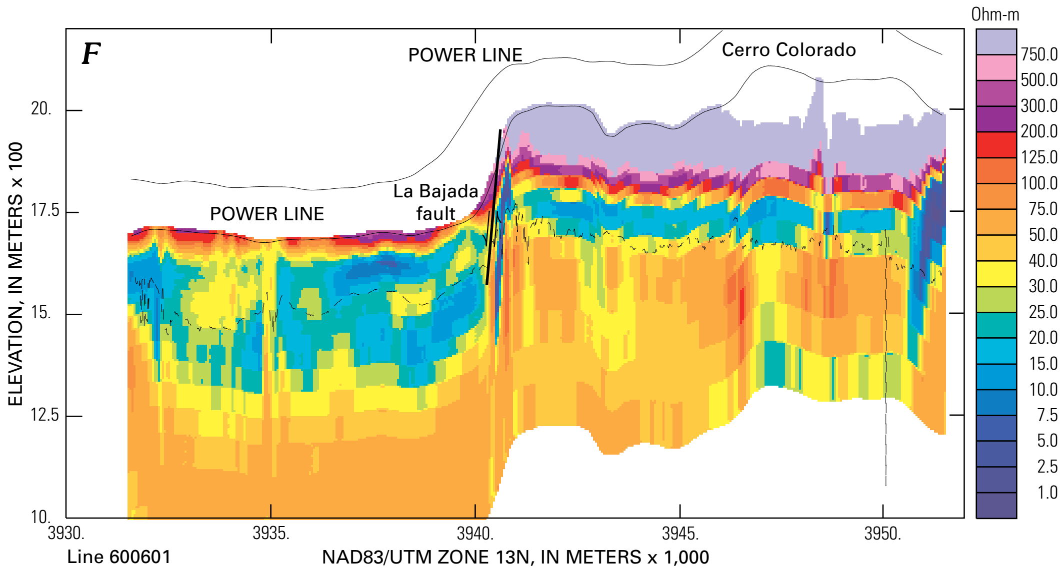
F
POWER LINE
Cerro Colorado
POWER LINE
La Bajada fault
ELEVATION, IN METERS x 100
20.
17.5
15.
12.5
10.
3930.
3935.
3940.
3945.
3950.
Line 600601
NAD83/UTM ZONE 13N, IN METERS x 1,000
Ohm-m
750.0
500.0
300.0
200.0
125.0
100.0
75.0
50.0
40.0
30.0
25.0
20.0
15.0
10.0
7.5
5.0
2.5
1.0

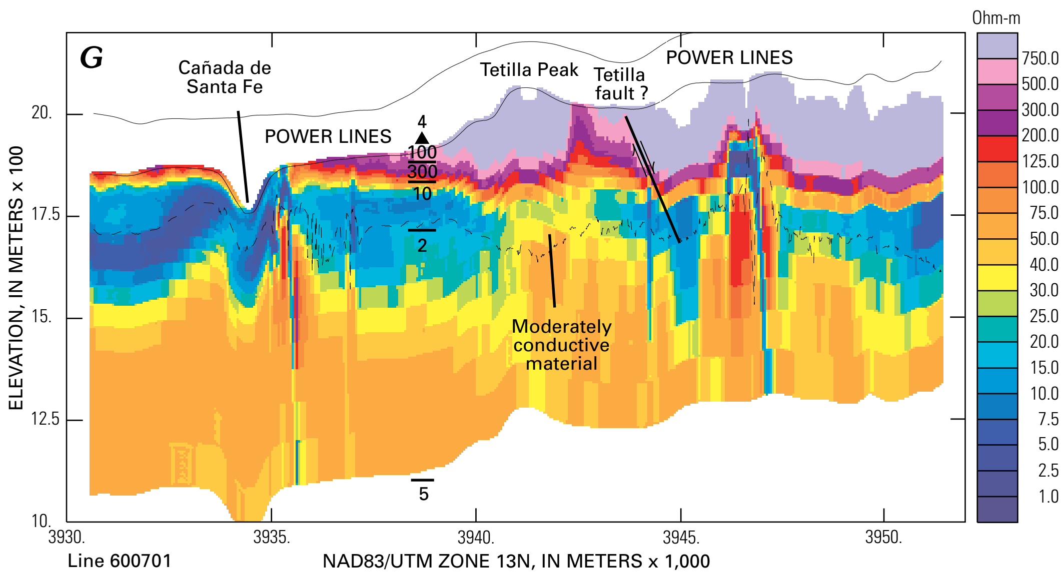
G
Cañada de Santa Fe
POWER LINES
Tetilla Peak
Tetilla fault ?
POWER LINES
4
100
300
10
2
5
Moderately conductive material
ELEVATION, IN METERS x 100
20.
17.5
15.
12.5
10.
3930.
3935.
3940.
3945.
3950.
Line 600701
NAD83/UTM ZONE 13N, IN METERS x 1,000
Ohm-m
750.0
500.0
300.0
200.0
125.0
100.0
75.0
50.0
40.0
30.0
25.0
20.0
15.0
10.0
7.5
5.0
2.5
1.0

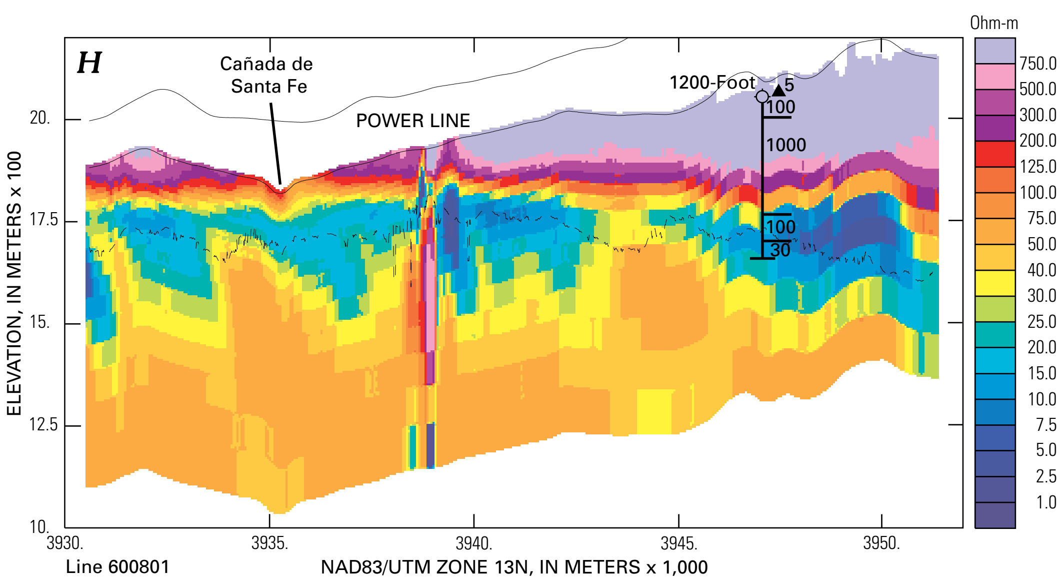
H
Cañada de Santa Fe
POWER LINE
1200-Foot
5
100
1000
100
30
ELEVATION, IN METERS x 100
20.
17.5
15.
12.5
10.
3930.
3935.
3940.
3945.
3950.
Line 600801
NAD83/UTM ZONE 13N, IN METERS x 1,000
Ohm-m
750.0
500.0
300.0
200.0
125.0
100.0
75.0
50.0
40.0
30.0
25.0
20.0
15.0
10.0
7.5
5.0
2.5
1.0

del Rio volcanic field. Resistivity values in the adjoining Cochiti Formation volcaniclastic sediments and axial gravels are also moderately high, in the range of 40–200 ohm-m.

The central La Bajada constriction area (that is, within the Santo Domingo Valley, fig. A4) has the lowest resistivities overall, and deposits in this area are generally less than 50 ohm-m resistivity. In the northern part of this area, a large area of lower resistivity coincides with a silt or clay lacustrine unit (F, near station AMT–2, figs. F12, F7) concealed within deposits of the upper Santa Fe Group. In the central part of the map area, higher resistivities correspond in part with ancestral Rio Grande axial-gravel deposits (C, M, fig. F12*C–F*). In areas lacking other subsurface information, boundaries within these deposits were inferred on the basis of grain size (fig. F12*C–F*); grain size, in turn, was established primarily on the basis of resistivity calibration (as previously described), but it was also constrained by local AMT soundings and lithologic well logs (Deszcz-Pan and others, 2000). The AMT soundings also helped us interpret the northern part of the survey area where thin (30–50 m) but strongly conductive, clay-rich sediments (<10 ohm-m) or rocks effectively blocked out those portions of the elevation-slice maps (fig. F12*C–F*) derived from the TDEM resistivity inversions. The TDEM data west of the La Bajada fault zone show that relatively lower resistivity values correspond with Santa Fe Group piedmont alluvium deposits, whereas relatively higher resistivity values correspond with axial gravel deposits of the ancestral Rio Grande. A large region of buried volcanic rock (V, fig. F12) in the subsurface of the Santo Domingo Basin is imaged by the modeled TDEM data. For example, aeromagnetic data (chapter D, this volume) indicate that a basaltic vent is buried just to the west of the Sanchez fault (magnetic anomaly C3, figs. F7, F11*D*), that abundant volcanic clasts contribute to the moderate resistivities just west of the Santa Cruz Springs well (magnetic anomaly C4, figs. F7, F11*D*), and that the rhyolite at the core of the W4 magnetic high (figs. F7, F11*B*) is at least 250 m thick and has resistivities well above 200 ohm-m. The apparent reduction in spatial size of the displayed resistivities for the deeper elevation slices (fig. F12*D–F*) is in part due to the depth-of-penetration limits of the TDEM survey. More detailed geologic interpretation and comparison of features seen in the TDEM models with geology and other geophysical data sets are discussed in chapter G (this volume).

Summary

Time-domain electromagnetic and magnetotelluric data were used to map changes in electrical resistivity with depth; these changes in resistivity are related to variations in rock types at depth; these variations in turn influence aquifers in the study area. These aquifers are part of the groundwater system hydraulically connected with the Rio Grande as it passes from the Española Basin into the Santo Domingo Basin.

1. In the area of the eastern Cerros del Rio volcanic field, the northern boundary of the Cerrillos uplift is constrained by magnetotelluric data reported in this chapter. Magnetotelluric soundings (figs. F4, F5) indicate that along a north-south line between audio-magnetotelluric stations 4 and 5, a 2 ohm-m conductor inferred to be the Cretaceous Mancos Shale is downdropped from a depth of 180 m at audio-magnetotelluric station 4 to a depth of 1,150 m beneath the surface at audio-magnetotelluric station This offset is evidence for 800 m of Tertiary structural relief at the north end of the Cerrillos uplift. The shallow Mancos Shale located at audio-magnetotelluric station 4, immediately south of Tetilla Peak, provides the farthest northwest constraint for the edge of the Cerrillos uplift and is consistent with the subsurface extent of the uplift based on gravity data.

2. Also in the area of the eastern Cerros del Rio volcanic field, the partly concealed Tetilla fault zone appears to form the western boundary of the east-dipping conductive Mancos Shale, based on time-domain electromagnetic results south of two northeast-trending power lines (fig. F11*F*). We do not see the same east-dipping conductive material in the terrane north of the power lines, near audio-magnetotelluric station 4 (fig. F11*D*), but rather we see minor breaks in what otherwise look like fairly flat-lying conductive layers. Moderately resistive material surrounded by moderately conductive material suggests some kind of structural block between audiomagnetotelluric stations 4 and 5 at a bearing of about N. 60° E. (fig. F12*B*). The structure of this block can also be seen north of audiomagnetotelluric station 4 (fig. F13*G*) and south of audiomagnetotelluric station 5 (fig. F13*H*). This moderately resistive block has resistivities similar to those of Santa Fe Group sediments.

3. In the northern part of the central La Bajada constriction, a large area of lower resistivity, defined by the time-domain electromagnetic survey results, coincides with a silt or clay lacustrine unit (region F, near audiomagnetotelluric station 2, figs. F12, F7) in the upper Santa Fe Group deposits. In the central part of the map, higher resistivities correspond in part with ancestral Rio Grande axial-gravel deposits (regions C and M, fig. F12).

4. The Saint Peters Dome block, in the footwall of the Pajarito fault zone, has a more complex stratigraphy than expected on the basis of the magnetotelluric results. Magnetotelluric soundings (fig. F6, magnetotelluric stations 12 and 17) provide additional constraints on the relative position of basement and thickness of Paleozoic, Mesozoic, and Tertiary sedimentary rocks across the Pajarito fault zone.

Figure F14 (following 2 pages). *A*, Depth to surface of resistive layer (>100 ohm-m) in the Cochiti Pueblo time-domain electromagnetic survey area, drawn on the basis of least-squares inversion. *B*, Elevation to base of surface resistive layer (>100 ohm-m) in the Cochiti Pueblo time-domain electromagnetic survey area, drawn on the basis of least-squares inversion.

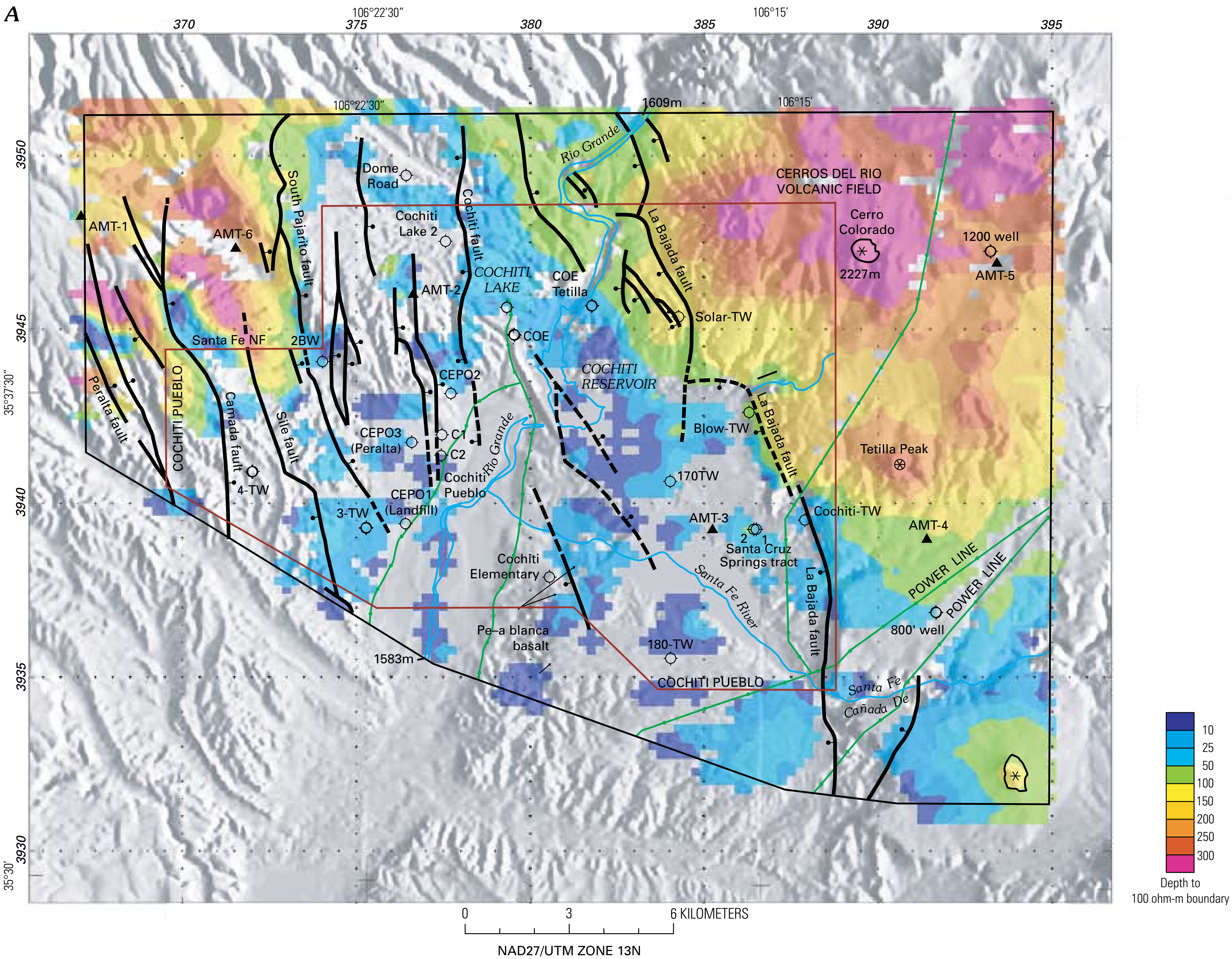
A
370
375
380
385
390
395
106°22'30"
106°15'
3950
3945
3940
3935
3930
35°37'30"
35°30'
1609m
Rio Grande
CERROS DEL RIO
VOLCANIC FIELD
Cerro
Colorado
2227m
1200 well
AMT-5
AMT-1
AMT-6
Dome
Road
Cochiti
Lake 2
South Pajarito fault
Cochiti fault
La Bajada fault
COCHITI
LAKE
COE
Tetilla
AMT-2
Solar-TW
COE
Santa Fe NF
2BW
CEPO2
COCHITI
RESERVOIR
Peralta fault
COCHITI PUEBLO
Canada fault
Sile fault
CEPO3
(Peralta)
C1
C2
Blow-TW
Tetilla Peak
4-TW
Cochiti
Pueblo
170TW
CEPO1
(Landfill)
3-TW
AMT-3
Cochiti-TW
AMT-4
2
1
Santa Cruz
Springs tract
Cochiti
Elementary
Santa Fe River
POWER LINE
POWER LINE
800' well
Pe–a blanca
basalt
180-TW
1583m
COCHITI PUEBLO
Santa Fe
Cañada De
10
25
50
100
150
200
250
300
Depth to
100 ohm-m boundary
0
3
6 KILOMETERS
NAD27/UTM ZONE 13N

B

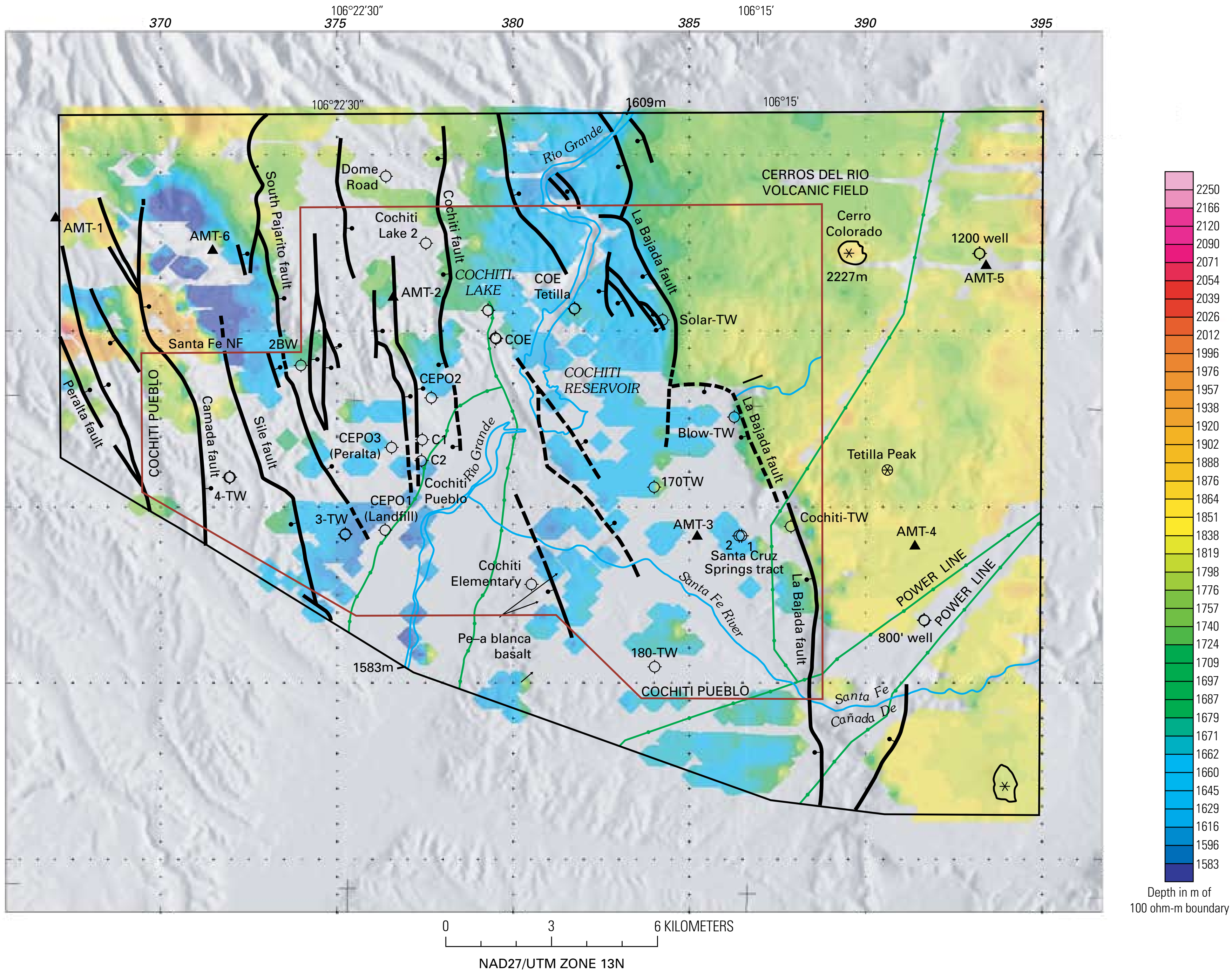
106°22'30"
106°15'
370
375
380
385
390
395
3950
3945
3940
3935
3930
35°37'30"
35°30'
1609m
CERROS DEL RIO
VOLCANIC FIELD
Cerro
Colorado
2227m
1200 well
AMT-5
AMT-1
AMT-6
AMT-2
AMT-3
AMT-4
Dome
Road
Cochiti
Lake 2
COCHITI
LAKE
COE
Tetilla
COE
Solar-TW
Santa Fe NF
2BW
CEPO2
COCHITI
RESERVOIR
Blow-TW
CEPO3
(Peralta)
C1
C2
Cochiti
Pueblo
170TW
4-TW
3-TW
CEPO1
(Landfill)
Cochiti-TW
Santa Cruz
Springs tract
Cochiti
Elementary
Tetilla Peak
POWER LINE
POWER LINE
800' well
Pe–a blanca
basalt
180-TW
1583m
COCHITI PUEBLO
COCHITI PUEBLO
Santa Fe
Cañada De
Rio Grande
Santa Fe River
Peralta fault
Camada fault
Sile fault
South Pajarito fault
Cochiti fault
La Bajada fault
0
3
6 KILOMETERS
NAD27/UTM ZONE 13N
2250
2166
2120
2090
2071
2054
2039
2026
2012
1996
1976
1957
1938
1920
1902
1888
1876
1864
1851
1838
1819
1798
1776
1757
1740
1724
1709
1697
1687
1679
1671
1662
1660
1645
1629
1616
1596
1583
Depth in m of
100 ohm-m boundary

References Cited

Bartolino, J.R., 1999, Introduction, *in* U.S. Geological Survey Middle Rio Grande Basin Study— 3d Annual Workshop, Albuquerque, New Mexico, February 24–25, 1999, Proceedings: U.S. Geological Survey Open-File Report 99–203, p. 2.

Bartolino, J.R., and Cole, J.C., 2002, Ground-water resources of the Middle Rio Grande Basin, New Mexico: U.S. Geological Survey Circular 1222, 132 p.

Bendat, J.S., and Piersol, A.G., 1971, Random data—Analysis and measurement procedures: New York, Wiley Interscience, 407 p.

Chamberlin, R.M., Jackson, P., and Connell, S.D., 1999, Field logs of borehole drilled for monitoring well at Dome Road site, Canada de Cochiti Grant, Sandoval County, New Mexico: New Mexico Bureau of Mines and Mineral Resources Open-file Report 444c, 30 p.

Clarke, J., Gamble, T.D., Goubau, W.M., Koch, R.H., and Miracky, R.F., 1983, Remote-reference magnetotellurics—Equipment and procedures: Geophysical Prospecting, v. 31, p. 149–170.

Cole, J.C., Grauch, V.J.S., Hudson, M.R., Maldonado, F., Minor, S.A., Sawyer, D.A., and Stone, B.D., 1999, Three-dimensional geologic modeling of the middle Rio Grande Basin, *in* Bartolino, J.R., ed., U.S. Geological Survey Middle Rio Grande Basin Study—3d Annual Workshop, Albuquerque, New Mexico, February 24–25, 1999, Proceedings: U.S. Geological Survey Open-File Report 99–203, p. 25–26.

Deszcz-Pan, M., Rodriguez, B.D., Doucette, J.P., Godbout, M., Williams, J.M., Sawyer, D.A., Stone, B.D., and Grauch, V.J.S., 2000, Digital airborne time domain electromagnetic data from surveys over Cochiti Pueblo, Rio Puerco, and Rio Rancho, New Mexico: U.S. Geological Survey Open-File Report 00–502 (CD-ROM).

Dobrin, M.D., and Savit, C.H., 1988, Introduction to geophysical prospecting (4th ed.): New York, McGraw-Hill, 867 p.

Ellis, R.G., 1998, Inversion of airborne electromagnetic data: Exploration Geophysics, v. 29, no. 1–2, p. 121–127.

Gamble, T.D., Goubau, W.M., and Clarke, J., 1979, Magnetotellurics with a remote magnetic reference: Geophysics, v. 44, no. 1, p. 53–68.

Grauch, V.J.S., 1999, Principal features of high-resolution aeromagnetic data collected near Albuquerque, New Mexico: New Mexico Geological Society 50th field conference, Albuquerque Geology, Guidebook, p. 115–118, 133–135.

Hearst, J.R., Nelson, P.H., and Paillet, F.L., 2000, Well logging for physical properties, 2d ed.: New York, John Wiley, 483 p.

Keller, G.V., 1987, Rock and mineral properties, *in* Nabighian, M.N., ed., Electromagnetic methods in applied geophysics, v. 1, Theory: Society of Exploration Geophysicists, p. 13–51.

Keller, G.V., and Frischknecht, F.C., 1966, Electrical methods in geophysical prospecting: New York, Pergamon Press, 517 p.

Liu, G., and Asten, M.A., 1993, Conductance-depth imaging of airborne TEM data: Exploration Geophysics, v. 24, no. 3–4, p. 655–662.

Nelson, P.H., and Anderson, L.A., 1992, Physical properties of ash flow tuff from Yucca Mountain, Nevada: Journal of Geophysical Research, v. 97, no. B5, p. 6823–6841.

Palacky, G.J., 1987, Resistivity characteristics of geologic targets, *in* Nabighian, M.N., ed., Electromagnetic methods in applied geophysics, v. 1, Theory: Society of Exploration Geophysicists, p. 53–129.

Palacky, G.J., and West, G.F., 1991, Airborne electromagnetic methods, *in* Nabighian, M.N., ed., Electromagnetic methods in applied geophysics, v. 2, Application: Society of Exploration Geophysicists, p. 811–879.

Smith, G.A., 2001, Development of a pyroclastic apron adjacent to rhyolite domes in a subsiding basin, upper Miocene Peralta Tuff, Jemez Mountains, New Mexico: New Mexico Museum of Natural History and Science, v. 18, p. 85–96.

Sternberg, B.K., Washburne, J.C., and Pellerin, L., 1988, Correction for the static shift in magnetotellurics using transient electromagnetic soundings: Geophysics, v. 53, p. 1459–1468.

Vozoff, K., 1972, The magnetotelluric method in the exploration of sedimentary basins: Geophysics, v. 37, p. 98–141.

Vozoff, K., 1991, The magnetotelluric method, *in* Nabighian, M.N., ed., Electromagnetic methods in applied geophysics, v. 2, Application, part B: Society of Exploration Geophysicists, Tulsa, Oklahoma, p. 641–711.

Wannamaker, P.E., Hohmann, G.W., and Ward, S.H., 1984, Magnetotelluric responses of three-dimensional bodies in layered earths: Geophysics, v. 49, no. 9, p. 1517–1533.

Wannamaker, P.E., Stodt, J.A., and Rijo, L., 1985, PW2D—Finite element program for solution of magnetotelluric responses of two-dimensional earth resistivity structure (user documentation): Salt Lake City, Utah, Earth Science Laboratory, University of Utah Research Institute, 40 p.

Williams, J.M., and Rodriguez, B.D., 2003, Magnetotelluric data in the southwest Española Basin, northern New Mexico: U.S. Geological Survey Open-File Report 03–199, 128 p.

Williams, J.M., Rodriguez, B.D., and Sampson, J.A., 2001, Magnetotelluric data in the Cochiti Pueblo area, New Mexico: U.S. Geological Survey Open-File Report 01–442, 66 p.

Published in the Central Region, Denver, Colo.
Manuscript approved for publication February 10, 2006
Graphics by authors
Photocomposition by Mari L. Kauffmann (Contractor, ATA Services)
Edited by Mary-Margaret Coates (Contractor, ATA Services)